LETTER

https://doi.org/10.1038/s41586-019-1535-2

Controlled modelling of human epiblast and amnion development using stem cells

Yi Zheng[1], Xufeng Xue[1], Yue Shao[1], Sicong Wang[1], Sajedeh Nasr Esfahani[1], Zida Li[1], Jonathon M. Muncie[2,3], Johnathon N. Lakins[2], Valerie M. Weaver[2,4,5], Deborah L. Gumucio[6] & Jianping Fu[1,6,7]*

Early human embryonic development involves extensive lineage diversification, cell-fate specification and tissue patterning[1]. Despite its basic and clinical importance, early human embryonic development remains relatively unexplained owing to interspecies divergence[2,3] and limited accessibility to human embryo samples. Here we report that human pluripotent stem cells (hPSCs) in a microfluidic device recapitulate, in a highly controllable and scalable fashion, landmarks of the development of the epiblast and amniotic ectoderm parts of the conceptus, including lumenogenesis of the epiblast and the resultant pro-amniotic cavity, formation of a bipolar embryonic sac, and specification of primordial germ cells and primitive streak cells. We further show that amniotic ectoderm-like cells function as a signalling centre to trigger the onset of gastrulation-like events in hPSCs. Given its controllability and scalability, the microfluidic model provides a powerful experimental system to advance knowledge of human embryology and reproduction. This model could assist in the rational design of differentiation protocols of hPSCs for disease modelling and cell therapy, and in high-throughput drug and toxicity screens to prevent pregnancy failure and birth defects.

In vitro cultured human embryos provide insights about the self-organizing properties and autonomy of early human development[4,5]. However, protocols for in vitro human embryo culture beyond the blastocyst stage remain suboptimal[4,5]. Furthermore, bioethical guidelines prohibit in vitro culture of human embryos beyond 14 days post-fertilization or reaching the onset of primitive streak (PS) development[6,7]. Human and mouse pluripotent stem cells in a developmental state similar to the epiblast have been used for modelling post-implantation development of human and mouse embryos[8–16]. Thus, models based on stem cells are an important ethical alternative to the use of natural conceptus, especially as they can model only part of the conceptus[17]. However, beyond phenomenological observations, some existing models suffer from unsatisfactory efficiency and reproducibility and are therefore suboptimal for mechanistic studies[8,9,11,15]. Recent efforts have made use of micropatterned surfaces[10,13] and microwell structures[14,16] to promote multicellular self-organization in controlled environments. Here we sought to use microfluidics to achieve a controllable model system to recapitulate developmental events reflecting epiblast and amniotic ectoderm development in the post-implantation human embryo.

The first morphological milestone of the post-implantation human embryo is the apical–basal polarization and lumenogenesis of the epiblast, resulting in the pro-amniotic cavity[4,5,18] (Fig. 1a). Lumenogenesis of the mouse epiblast is shown to occur after the naive-to-primed pluripotency transition in the mouse epiblast[18]. Thus, we first sought to reproducibly generate lumenal cysts using primed hPSCs. We developed a microfluidic device containing three parallel channels, partitioned by evenly spaced supporting posts (Fig. 1b, Extended Data Fig. 1a–c and Methods). The central gel channel is preloaded with Geltrex, whereas the other two open channels serve as a cell-loading channel and a chemical-induction channel, respectively. Geltrex contraction during gelation leads to formation of concave gel pockets between supporting posts (Extended Data Fig. 1d). Single H9 human embryonic stem (ES) cells injected into the cell-loading channel settle into gel pockets and subsequently cluster (Extended Data Fig. 1d). At 18 h after cell seeding (designated as $t = 0$ h), the culture medium is switched to basal medium, comprising Essential 6 medium supplemented with FGF2. From $t = 0$ h onwards, nascent cavities containing ezrin$^+$ apical membranes emerge[5,19] (Extended Data Fig. 1e, f, Fig. 1b). By $t = 36$ h, E-cadherin$^+$ epithelial sacs containing a single central lumen are developed, enclosed by a single layer of columnar, OCT4$^+$NANOG$^+$SOX2$^+$ epiblast-like cells (EPILCs) (Fig. 1b, c, Extended Data Fig. 1e–l and Supplementary Video 1), reminiscent of the pro-amniotic cavity formed in the epiblast at Carnegie stage 5a[4,5,18]. During lumenogenesis, epiblast-like cysts expand in size while increasing cell number (Extended Data Fig. 1f, i–k). Development of epiblast-like cysts is not sensitive to inhibition of Wnt, BMP or TGF-β signalling or apoptosis (Extended Data Fig. 1m, n).

In the post-implantation human embryo, formation of the pro-amniotic cavity in the epiblast is followed by dorsal–ventral patterning, resolving the epiblast into a bipolar embryonic sac, with squamous amniotic ectoderm and epiblast at the prospective dorsal and ventral poles, respectively (Fig. 1a). Formation of the bipolar embryonic sac precedes the gastrulation of the epiblast, during which the primitive streak emerges at the prospective posterior end of the epiblast (PrePS-EPI) (Fig. 1a). We tested whether epiblast-like cysts could recapitulate events similar to dorsal–ventral patterning of the epiblast. Recent studies of the post-implantation cynomolgus macaque (*Macaca fascicularis*) and mouse embryos reveal strong BMP activity in the amniotic ectoderm[20,21]. Our previous study also demonstrated a requirement for BMP signalling in amniogenic differentiation of hPSCs[12]. Thus, we aimed to induce dorsal–ventral patterning of epiblast-like cysts by supplementing BMP4 in the induction channel from $t = 0$ h onwards (Fig. 1b and Extended Data Fig. 2a). At $t = 36$ h, 92% of cysts differentiated into asymmetrical, E-cadherin$^+$ sacs, with a single layer of flattened, amniotic ectoderm-like cells (AMLCs) at the pole exposed to BMP4, and a stratified, epiblast-like epithelium at the other pole, resembling the human asymmetric embryonic sac before the onset of gastrulation at 7–12 days post-fertilization (Carnegie stage 5b–5c) (Fig. 1d, Extended Data Fig. 2b–d and Supplementary Video 2). Immunofluorescence analyses confirmed nuclear staining of phosphorylated SMAD1–SMAD5 (pSMAD1/5), a downstream target of BMP signalling, in AMLCs (Extended Data Fig. 2e). TFAP2A, a putative amniotic ectoderm marker[12], is exclusively expressed in AMLCs (Fig. 1d, Extended Data Fig. 2e). CDX2 is thought to be a marker for both amniotic ectoderm[12] and posterior primitive streak[22], whereas brachyury

[1]Department of Mechanical Engineering, University of Michigan, Ann Arbor, MI, USA. [2]Department of Surgery, Center for Bioengineering and Tissue Regeneration, University of California, San Francisco, San Francisco, CA, USA. [3]Graduate Program in Bioengineering, University of California, San Francisco and University of California, Berkeley, San Francisco, CA, USA. [4]Department of Bioengineering and Therapeutic Sciences, Eli and Edythe Broad Center of Regeneration Medicine and Stem Cell Research, University of California, San Francisco, San Francisco, CA, USA. [5]Department of Radiation Oncology, Helen Diller Family Comprehensive Cancer Center, University of California, San Francisco, San Francisco, CA, USA. [6]Department of Cell and Developmental Biology, University of Michigan Medical School, Ann Arbor, MI, USA. [7]Department of Biomedical Engineering, University of Michigan, Ann Arbor, MI, USA. *e-mail: jpfu@umich.edu

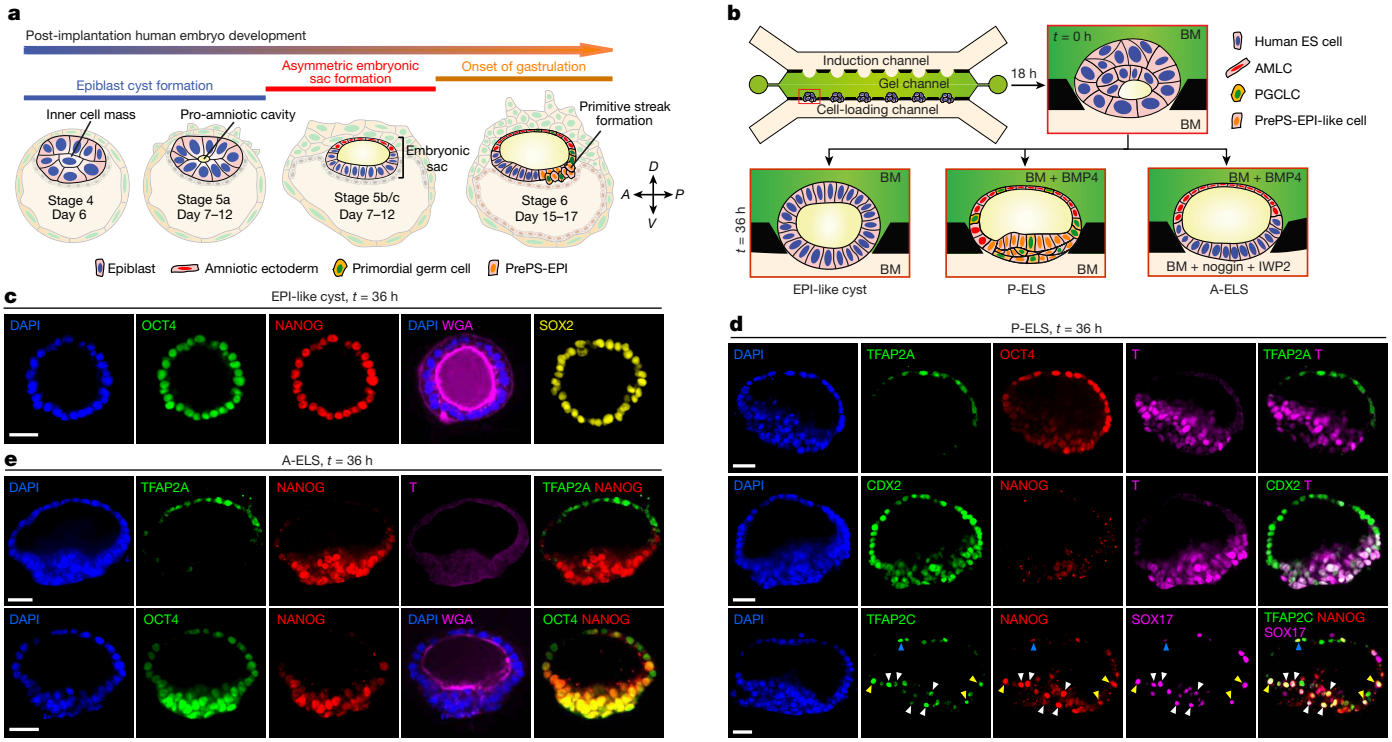

Fig. 1 | Microfluidic modelling of human epiblast and amnion development. a, Mid-sagittal view of the post-implantation human embryo. The inner cell mass of the blastocyst first polarizes and forms the epiblast cyst containing the pro-amniotic cavity. The epiblast cyst then resolves into a patterned embryonic sac, with squamous amniotic ectoderm at one pole and columnar epiblast at the other. The primitive streak soon emerges at the prospective posterior end of the epiblast. Primordial germ cells are thought to arise during asymmetric embryonic sac development before gastrulation. Carnegie stages and embryonic days are indicated. **b**, Microfluidic generation of epiblast-like cyst, anteriorized embryonic-like sac (A-ELS) and posteriorized embryonic-like sac (P-ELS). Human ES cells seeded into pre-formed gel pockets at $t = -18$ h initiate lumenogenesis spontaneously. A-ELS and P-ELS are obtained at $t = 36$ h by supplementing the medium with growth factors, morphogens and/or antagonists via the cell-loading and/or induction channels as indicated. **c**, Representative confocal micrographs showing epiblast (EPI)-like cysts at $t = 36$ h stained for OCT4, NANOG and SOX2. Plasma membrane is stained with fluorescently labelled wheat germ agglutinin (WGA). Experiments were repeated five times with similar results. **d**, Representative confocal micrographs showing P-ELS at $t = 36$ h stained for TFAP2A, OCT4 and T (top); CDX2, NANOG and T (middle); TFAP2C, NANOG and SOX17 (bottom). $TFAP2C^+SOX17^+$ human PGC-like cells are marked by colour-coded arrowheads to indicate spatial localizations (blue, amniotic ectoderm-like compartment; yellow, amniotic ectoderm–epiblast junction; white, PrePS-EPI-like compartment). Experiments were repeated five times with similar results. **e**, Representative confocal micrographs showing A-ELS at $t = 36$ h stained for TFAP2A, NANOG and T (top); OCT4 and NANOG (bottom). Experiments were repeated four times with similar results. In **c**–**e**, nuclei were counterstained with DAPI. Scale bars, 40 μm. BM, basal medium.

(also known as T-box transcription factor or T) is a primitive streak marker[23] and is expressed transiently in the *M. fascicularis* amniotic ectoderm[21] and during amniogenic differentiation of hPSCs[12,15]. At $t = 24$ h, incipient AMLCs express NANOG, CDX2 and T (Extended Data Fig. 2f), reflecting a fate transition from pluripotent epiblast to amniotic ectoderm. Thereafter, whereas incipient AMLCs acquire squamous morphology and lose NANOG and T expression, CDX2 and T expression spreads into the epiblast-like compartment (Extended Data Fig. 2f). At $t = 36$ h, T is exclusively expressed in EPILCs, whereas NANOG is only retained at the centre of the T^+, epiblast-like pole (Fig. 1d, Extended Data Fig. 2f). Because EPILCs are $CDX2^+T^+$, but are losing NANOG—suggesting a PrePS-EPI phenotype exiting from pluripotency[21,22]—these asymmetric sacs are hereafter referred to as posteriorized embryonic-like sacs (P-ELS). From $t = 36$ h onwards, EPILCs start to emigrate only from the epiblast-like pole, leading to cyst collapse (Supplementary Video 2). Prolonged culture to $t = 72$ h was occasionally successful; in such cases, continuous thinning of AMLCs was evident (Extended Data Fig. 2g, h), and GATA3, another putative amniotic ectoderm maker[12], appeared exclusively in $TFAP2A^+$ AMLCs (Extended Data Fig. 2g). OCT4 showed strong nuclear staining in all cells of P-ELS (Fig. 1d, Extended Data Fig. 2g), and in situ hybridization of *BMP4* and *AXIN2* mRNA revealed very weak expression of *AXIN2* in P-ELS and robust *BMP4* expression in AMLCs (Extended Data Fig. 2i–k). Prominent *BMP4* expression is also evident in *M. fascicularis* amniotic ectoderm at embryonic day (E)11–E12[21].

In the E11–E12 *M. fascicularis* embryo, T^+ gastrulating cells emerge in the PrePS-EPI, whereas the anterior epiblast remains $OCT4^+NANOG^+$, but T^- (ref. [21]). In the E6.5 mouse embryo, Wnt and NODAL antagonists secreted by the anterior visceral endoderm restrict the primitive streak formation to the PrePS-EPI[2]. Of note, the Wnt antagonist DKK1 and the BMP antagonist CER1 are evident in the anterior visceral endoderm of the E11–E12 *M. fascicularis* embryo[21]. Thus, to prevent gastrulating cell development, IWP2 (an inhibitor of Wnt-ligand secretion) and noggin (a BMP antagonist) were added to the cell-loading channel in addition to BMP4 in the induction channel (Fig. 1b, Extended Data Fig. 3a). BMP4 stimulation still elicits patterning in 96% of cysts at $t = 36$ h to confer amniotic ectoderm-like fate on cells that are directly exposed to BMP4 (Fig. 1e, Extended Data Fig. 3b–d). However, compared with P-ELS, the epiblast-like pole appears more organized and is $OCT4^+NANOG^+$, but T^- (Fig. 1e, Extended Data Fig. 3e, f). These events reflect aspects of the formation of the anteriorized embryonic sac; we therefore designate these structures anteriorized embryonic-like sacs (A-ELS).

In the *M. fascicularis* embryo, primordial germ cells (PGCs), the precursors of sperm and egg, are thought to arise during embryonic sac formation before gastrulation[21,24] (Fig. 1a, Extended Data Fig. 4a). We examined whether human PGC-like cells (hPGCLCs) would develop in P-ELS. $TFAP2C^+SOX17^+$ cells have been identified as early-stage hPGCLCs[21,25,26]. Indeed, $TFAP2C^+SOX17^-$ and $SOX17^+$ $TFAP2C^-$ cells, presumably in the process of hPGCLC specification, as well as

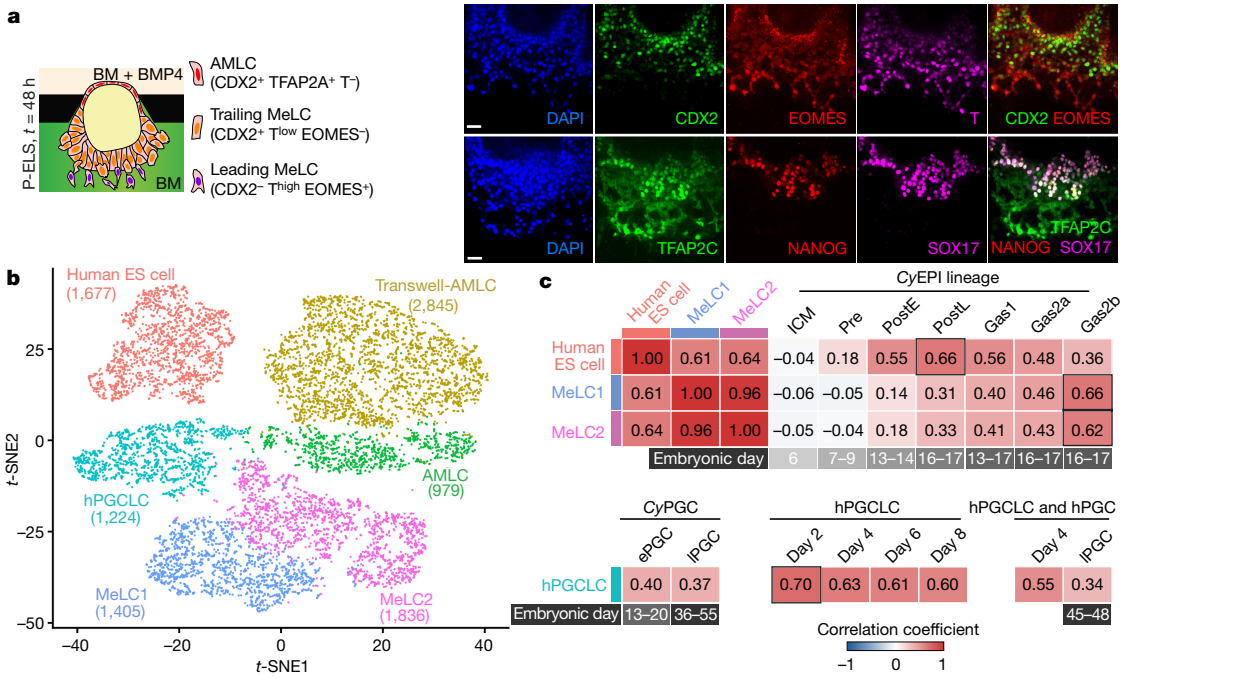

	Human ES cell	MeLC1	MeLC2	ICM	Pre	PostE	PostL	Gas1	Gas2a	Gas2b
Human ES cell	1.00	0.61	0.64	−0.04	0.18	0.55	0.66	0.56	0.48	0.36
MeLC1	0.61	1.00	0.96	−0.06	−0.05	0.14	0.31	0.40	0.46	0.66
MeLC2	0.64	0.96	1.00	−0.05	−0.04	0.18	0.33	0.41	0.43	0.62
Embryonic day				6	7–9	13–14	16–17	13–17	16–17	16–17

	CyPGC ePGC	CyPGC lPGC	hPGCLC Day 2	hPGCLC Day 4	hPGCLC Day 6	hPGCLC Day 8	hPGCLC and hPGC Day 4	hPGCLC and hPGC lPGC
hPGCLC	0.40	0.37	0.70	0.63	0.61	0.60	0.55	0.34
Embryonic day	13–20	36–55						45–48

Fig. 2 | Single-cell transcriptomic analysis of posteriorized embryonic-like sac. a, Left, schematic of P-ELS at $t = 48$ h. Right, representative confocal micrographs showing staining for CDX2, EOMES and T (top); TFAP2C, NANOG and SOX17 (bottom). Experiments were repeated three times with similar results. Scale bars, 40 μm. **b**, *t*-SNE plot generated from scRNA-seq data of a total of 9,966 cells, revealing six distinct, colour-coded cell populations (human ES cell, Transwell-AMLC, AMLC, hPGCLC, MeLC1 and MeLC2; see Extended Data Fig. 8). Cell numbers of each population are indicated. **c**, Heat map of correlation coefficients among indicated cell types including those reported by others[21,23,25,26]. Comparisons between human ES cell, MeLC1 and MeLC2 clusters and *M. fascicularis* (*Cy*) epiblast lineages are based on ontogenic genes identified for *M. fascicularis* epiblast (651 in common out of 776)[23]. Comparisons between hPGCLC cluster, *M. fascicularis* PGC, hPGCLC and hPGC are based on ontogenic *Cy*PGC genes (477 in common out of 544)[21]. Correlation coefficient is calculated using averages of log-transformed expression of common genes. *M. fascicularis* epiblast (*Cy*EPI) lineages: ICM, inner cell mass; Pre, pre-implantation epiblast; PostE and PostL, post-implantation early and late epiblast, respectively; Gas1, Gas2a, Gas2b, gastrulating cells. For *Cy*PGC and hPGC: ePGC, early *Cy*PGC; lPGC, late gonadal *Cy*PGC or hPGC. Embryonic days are indicated for *Cy*EPI lineages, *Cy*PGC and hPGC below the heat maps. For hPGCLCs (reported in refs. [25,26]), culture day is indicated. Coloured bars above and besides the heat maps indicate cell types in P-ELS. All genes are listed in Supplementary Table 1.

TFAP2C$^+$SOX17$^+$ and TFAP2C$^+$NANOG$^+$SOX17$^+$ hPGCLCs were detected at $t = 24$ h in a scattered fashion throughout the entire P-ELS (Fig. 1d, Extended Data Fig. 4b–d). At $t = 24$ h, both TFAP2C$^+$SOX17$^+$ and TFAP2C$^+$NANOG$^+$SOX17$^+$ hPGCLCs were predominantly located in the incipient amniotic ectoderm-like compartment (Extended Data Fig. 4b, d). Over time, hPGCLCs accumulated at the junction of amniotic ectoderm-like and epiblast-like compartments and in the epiblast-like pole. At $t = 36$ h, hPGCLCs, which were prevalent in the PrePS-EPI-like pole, were also BLIMP1$^+$, suggesting a fully committed stage to germline cell development (Fig. 1d, Extended Data Fig. 4b, d). At $t = 72$ h, no TFAP2C$^+$ or NANOG$^+$ cells were detected in the amniotic ectoderm-like compartment (Extended Data Fig. 2g). We further examined T expression, as T is essential for mouse PGC specification[27] and is associated with hPGCLC specification[25,26]. T was detected only in a subset of TFAP2C$^+$SOX17$^+$ hPGCLCs in P-ELS at $t = 36$ h (Extended Data Fig. 4e). Treatment of P-ELS with the GP130 inhibitor SC144 did not affect hPGCLC specification (Extended Data Fig. 4f). No TFAP2C$^+$SOX17$^+$ hPGCLCs were detected in A-ELS, consistent with data from the *M. fascicularis* embryo[21] and existing literature showing requirements for BMP and Wnt signalling for hPGCLC specification[24].

We also generated epiblast-like cysts, P-ELS and A-ELS from different primed human ES cell lines and a human induced-PSC line (Extended Data Fig. 5). We further confirmed specification of hPGCLCs in P-ELS using these hPSC lines (Extended Data Fig. 5b).

BMP and TGF-β–activin signalling have been suggested to confer characteristics of posterior[28] and anterior[29] primitive streak-cell phenotypes on hPSCs, respectively; however, in P-ELS, EPILCs directly exposed to BMP4 consistently give rise to AMLCs before EPILCs at the opposite pole display a posterior primitive streak-cell phenotype (Fig. 1d). To elucidate the roles of developmental signals, WNT3A or activin A was supplemented into the induction channel, with or without BMP4 (Extended Data Fig. 6). WNT3A alone gave rise to columnar epiblast-like cysts containing OCT4$^+$NANOG$^+$, CDX2$^-$EOMES$^-$T$^-$ EPILCs (Extended Data Fig. 6a). Activin A alone generated cysts containing OCT4$^+$NANOG$^+$ EPILCs intermixed with EOMES$^+$T$^+$CDX2$^-$ anterior primitive streak-like cells (Extended Data Fig. 6b). WNT3A and BMP4 together resulted in P-ELS (Extended Data Fig. 6c), whereas activin A and BMP4 together generated asymmetric sacs containing TFAP2A$^+$CDX2$^+$ AMLCs at the pole directly facing activin A–BMP4 stimulation and EOMES$^+$T$^+$CDX2$^-$ anterior primitive streak-like cells at the opposite pole (Extended Data Fig. 6d). Together, these data suggest that WNT3A is dispensable for embryonic-like sac formation and confirm the ability of activin signalling to confer an anterior primitive streak-like cell phenotype on the PrePS-EPI-like cells (PrePS-EPILCs).

Because cell dissemination in P-ELS resembles cell movement during gastrulation of the epiblast, we investigated this event further. To this end, BMP4 was supplemented into the cell loading channel from $t = 0$ h onwards (Fig. 2a, Extended Data Fig. 7a). The PrePS-EPI-like pole became thickened before cell dissemination (Extended Data Fig. 7a–c and Supplementary Video 3). From $t = 36$ h onwards, individual cells began to migrate away from the PrePS-EPI-like pole and morphologically acquired a mesenchymal phenotype (Extended Data Fig. 7b). At $t = 48$ h, variable levels of T, EOMES and CDX2 were detected in migrating cells; leading cells showed high intensity T staining (T^{high}) and upregulated EOMES (EOMES$^+$) and N-cadherin (N-cadherin$^+$), but not CDX2, whereas trailing cells exhibited CDX2

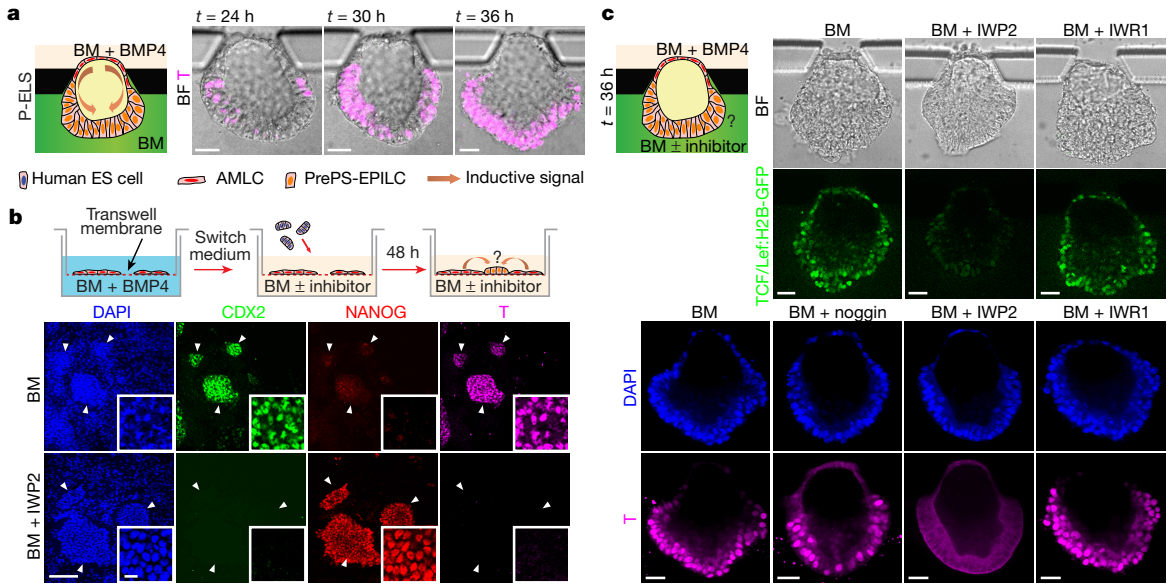

Fig. 3 | Amniotic ectoderm-like cells trigger mesoderm induction in posteriorized embryonic-like sac involving Wnt signalling. **a**, Schematic of microfluidic setting for mesoderm induction in P-ELS. Representative composite images show staining of T at indicated time points. Experiments were repeated three times with similar results. Scale bars, 40 μm. **b**, Co-culture assay of AMLCs and human ES cells. Human ES cells were first differentiated into AMLCs by culturing in basal medium supplemented with BMP4 for 48 h. Culture medium was then switched to fresh basal medium or basal medium with IWP2. At this point, undifferentiated human ES cells were seeded onto Transwell membranes and co-cultured with AMLCs for another 48 h. Representative confocal micrographs showing staining for CDX2, NANOG and T. Nuclei were counterstained with DAPI. Insets show magnified views of one of the human ES cell colonies marked by white arrowheads. Experiments were repeated three times with similar results. Scale bars, 160 μm (main panels) and 10 μm (insets). **c**, Top, live imaging with TCF/Lef:H2B-GFP human ES cell reporter line to track Wnt–β-catenin signalling dynamics during embryonic-like sac development with or without Wnt inhibitors IWP2 or IWR1 supplemented into the induction channel as indicated. Bottom, representative confocal micrographs showing embryonic-like sacs obtained at $t = 36$ h when indicated antagonists are supplemented into the induction channel. Cells were stained for T. Nuclei were counterstained with DAPI. Experiments were repeated four times with similar results. Scale bars, 40 μm.

staining ($CDX2^+$) and low-intensity T staining (T^{low}), but did not express EOMES or N-cadherin (Fig. 2a, Extended Data Fig. 7d). At $t = 48$ h, NANOG expression was restricted to $TFAP2C^+SOX17^+$ hPGCLCs, which began to migrate away from the PrePS-EPI-like compartment as clusters (Fig. 2a, Extended Data Fig. 7e). To induce the anterior primitive streak-cell phenotype, activin A was supplemented into the induction channel (Extended Data Fig. 7f). At $t = 48$ h, compared with posterior primitive streak-cell phenotype, anterior primitive streak-like cells appeared more migratory, with leading cells $EOMES^{high}$ and N-$cadherin^{high}$ (Extended Data Fig. 7g, h). NANOG expression was restricted to $TFAP2C^+SOX17^+$ hPGCLCs, which were still contained in embryonic-like sacs (Extended Data Fig. 7i). A distinct $SOX17^+TFAP2C^-NANOG^-$ cell population was evident in trailing cells, which were presumably in the process of endoderm specification[30] (Extended Data Fig. 7i).

Using single-cell RNA sequencing analysis (scRNA-seq), we further studied P-ELS obtained at $t = 48$ h, together with human ES cells and AMLCs derived using a Transwell method (Transwell-AMLC; Extended Data Fig. 8a). In the *t*-distributed stochastic neighbour embedding (*t*-SNE) plot, six distinct cell clusters emerged and were annotated as human ES cell, Transwell-AMLC, AMLC, hPGCLC, mesoderm-like cell (MeLC) 1 and MeLC2, on the basis of lineage markers (Fig. 2b, Extended Data Fig. 8b). Notably, in addition to *SOX17*, *TFAP2C*, *BLIMP1* (also known as *PRDM1*) and *NANOG*, the hPGCLC cluster expressed *NANOS3* (Extended Data Fig. 8b–f). MeLC1 and MeLC2 clusters corresponded to $T^{high}EOMES^+$ leading cells and $T^{low}EOMES^-$ trailing cells in P-ELC, respectively (Extended Data Fig. 8b–d). Genes upregulated in the MeLC2 cluster relative to the MeLC1 cluster were enriched for those associated with 'body pattern specification/organ morphogenesis' (Extended Data Fig. 8c–e), including *HOXA10*, *HOXB6*, *HOXB8* and *HOXB9*, suggesting a later developmental stage. Genes upregulated in the MeLC1, hPGCLC and AMLC clusters relative to the human ES cell cluster exhibit marked enrichments for 'embryonic morphogenesis', 'regulation of cell proliferation/cell motility' and 'cell migration/protein localization', respectively, whereas the downregulated genes are enriched for 'stem cell population maintenance' (Extended Data Fig. 8e). Expression of ectoderm markers *PAX6*, *SOX1* and *OTX2* or endoderm markers *SOX17*, *CXCR4*, *CER1* and *FOXA2* was not detected in the MeLC1 cluster (Extended Data Fig. 8f). Transcriptomic profiles of AMLC and Transwell-AMLC clusters were similar, and could only be distinguished using the *t*-SNE2 axis (Extended Data Fig. 8b–g). On the basis of ontogenic *M. fascicularis* epiblast genes[22], human ES cell and MeLC1–MeLC2 clusters showed the closest correlations with post-implantation late *M. fascicularis* epiblast and gastrulating cells at E16–E17, respectively (Fig. 2c, Extended Data Fig. 8g). The hPGCLC cluster exhibited the closest correlation with early-stage hPGCLCs on the basis of ontogenic *M. fascicularis* PGC genes[21] (Fig. 2c, Extended Data Fig. 8g).

Mouse gastrulation is initiated at the proximal, posterior end of the mouse epiblast by a convergence of BMP–Wnt–NODAL signalling, established through reciprocal interactions between the mouse epiblast and the juxtaposed extraembryonic ectoderm. The trophectoderm, the counterpart of extraembryonic ectoderm in the post-implantation human embryo, however, is physically separated from the epiblast by the amniotic ectoderm. We thus sought to study the role of AMLCs in triggering gastrulation-like events in P-ELS. T expression always emerged first in regions of the PrePS-EPI-like compartment adjacent to the amniotic ectoderm-like compartment before its propagation to the rest of the PrePS-EPI-like compartment (Fig. 3a, Extended Data Fig. 9a–e and Supplementary Video 4). We further examined inductive roles of Transwell-AMLCs (Fig. 3b, Extended Data Fig. 9f–i). Even without exogenous inductive factors, human ES cells co-cultured with Transwell-AMLCs for 48 h would exit from pluripotency and display a posterior primitive streak-cell phenotype (Fig. 3b, Extended Data Fig. 9h, i). $TFAP2C^+NANOG^+SOX17^+$ hPGCLCs are evident in human ES cells, but not in Transwell-AMLCs, after 48 h of

co-culture (Extended Data Fig. 9i). Differentiation of posterior primitive streak-like cells is inhibited, however, when IWP2 is supplemented into the Transwell co-culture system (Fig. 3b, Extended Data Fig. 10a), suggesting the involvement of Wnt signalling in inductive effects of Transwell-AMLCs. We further used a TCF/Lef:H2B-GFP human ES cell reporter line to generate P-ELS, confirming active Wnt–β-catenin signalling in the PrePS-EPI-like compartment (Fig. 3c, Extended Data Fig. 10b). Of note, PrePS-EPI-like cell development is completely inhibited by IWP2 supplemented in the induction channel, but not by noggin or IWR1, a specific inhibitor targeting turnover of AXIN2, a member of the β-catenin destruction complex, suggesting that initiation of gastrulation-like events in PrePS-EPI-like cells might be independent of AXIN2 (Fig. 3c, Extended Data Fig. 10b). Supporting this notion, our in situ hybridization data (Extended Data Fig. 2i) and scRNA-seq data (Extended Data Fig. 8f) show very weak expression of *AXIN2* in P-ELS. Prolonged culture of P-ELS to $t = 48$ h under IWR1 treatment confirms that IWR1 does not affect the progressive development of P-ELS (Extended Data Fig. 10c).

In this study, we report a hPSC-based microfluidic model to recapitulate successive key early human post-implantation developmental landmarks. We further show that AMLCs have a critical role both in triggering the onset of gastrulation-like events and in the specification of hPGCLCs. Our data also show that AMLCs and hPGCLCs would arise during the development of the asymmetric embryonic-like sac from primed hPSCs, providing a new perspective on the fluidity of pluripotency phases associated with hPSCs and probably also human epiblast.

Online content

Any methods, additional references, Nature Research reporting summaries, source data, extended data, supplementary information, acknowledgements, peer review information; details of author contributions and competing interests; and statements of data and code availability are available at https://doi.org/10.1038/s41586-019-1535-2.

Received: 30 May 2018; Accepted: 6 August 2019;
Published online: 11 September 2019

1. O'Rahilly, R. & Müller, F. *Developmental Stages in Human Embryos*. (Carnegie Institution of Washington, 1987).
2. Rossant, J. Mouse and human blastocyst-derived stem cells: vive les differences. *Development* **142**, 9–12 (2015).
3. Davidson, K. C., Mason, E. A. & Pera, M. F. The pluripotent state in mouse and human. *Development* **142**, 3090–3099 (2015).
4. Deglincerti, A. et al. Self-organization of the in vitro attached human embryo. *Nature* **533**, 251–254 (2016).
5. Shahbazi, M. N. et al. Self-organization of the human embryo in the absence of maternal tissues. *Nat. Cell Biol.* **18**, 700–708 (2016).
6. Daley, G. Q. et al. Setting global standards for stem cell research and clinical translation: the 2016 ISSCR guidelines. *Stem Cell Reports* **6**, 787–797 (2016).
7. Hyun, I., Wilkerson, A. & Johnston, J. Embryology policy: revisit the 14-day rule. *Nature* **533**, 169–171 (2016).
8. ten Berge, D. et al. Wnt signaling mediates self-organization and axis formation in embryoid bodies. *Cell Stem Cell* **3**, 508–518 (2008).
9. van den Brink, S. C. et al. Symmetry breaking, germ layer specification and axial organisation in aggregates of mouse embryonic stem cells. *Development* **141**, 4231–4242 (2014).
10. Warmflash, A., Sorre, B., Etoc, F., Siggia, E. D. & Brivanlou, A. H. A method to recapitulate early embryonic spatial patterning in human embryonic stem cells. *Nat. Methods* **11**, 847–854 (2014).
11. Harrison, S. E., Sozen, B., Christodoulou, N., Kyprianou, C. & Zernicka-Goetz, M. Assembly of embryonic and extra-embryonic stem cells to mimic embryogenesis in vitro. *Science* **356**, eaal1810 (2017).
12. Shao, Y. et al. Self-organized amniogenesis by human pluripotent stem cells in a biomimetic implantation-like niche. *Nat. Mater.* **16**, 419–425 (2017).
13. Xue, X. et al. Mechanics-guided embryonic patterning of neuroectoderm tissue from human pluripotent stem cells. *Nat. Mater.* **17**, 633–641 (2018).
14. Beccari, L. et al. Multi-axial self-organization properties of mouse embryonic stem cells into gastruloids. *Nature* **562**, 272–276 (2018).
15. Shao, Y. et al. A pluripotent stem cell-based model for post-implantation human amniotic sac development. *Nat. Commun.* **8**, 208 (2017).
16. Rivron, N. C. et al. Blastocyst-like structures generated solely from stem cells. *Nature* **557**, 106–111 (2018).
17. Rivron, N. et al. Debate ethics of embryo models from stem cells. *Nature* **564**, 183–185 (2018).
18. Shahbazi, M. N. et al. Pluripotent state transitions coordinate morphogenesis in mouse and human embryos. *Nature* **552**, 239–243 (2017).
19. Taniguchi, K. et al. Lumen formation is an intrinsic property of isolated human pluripotent stem cells. *Stem Cell Reports* **5**, 954–962 (2015).
20. Dobreva, M. P. et al. Periostin as a biomarker of the amniotic membrane. *Stem Cells Int.* **2012**, 987185 (2012).
21. Sasaki, K. et al. The germ cell fate of cynomolgus monkeys is specified in the nascent amnion. *Dev. Cell* **39**, 169–185 (2016).
22. Nakamura, T. et al. A developmental coordinate of pluripotency among mice, monkeys and humans. *Nature* **537**, 57–62 (2016).
23. Bernardo, A. S. et al. BRACHYURY and CDX2 mediate BMP-induced differentiation of human and mouse pluripotent stem cells into embryonic and extraembryonic lineages. *Cell Stem Cell* **9**, 144–155 (2011).
24. Kobayashi, T. et al. Principles of early human development and germ cell program from conserved model systems. *Nature* **546**, 416–420 (2017).
25. Irie, N. et al. SOX17 is a critical specifier of human primordial germ cell fate. *Cell* **160**, 253–268 (2015).
26. Sasaki, K. et al. Robust in vitro induction of human germ cell fate from pluripotent stem cells. *Cell Stem Cell* **17**, 178–194 (2015).
27. Aramaki, S. et al. A mesodermal factor, T, specifies mouse germ cell fate by directly activating germline determinants. *Dev. Cell* **27**, 516–529 (2013).
28. Mendjan, S. et al. NANOG and CDX2 pattern distinct subtypes of human mesoderm during exit from pluripotency. *Cell Stem Cell* **15**, 310–325 (2014).
29. Gadue, P., Huber, T. L., Paddison, P. J. & Keller, G. M. Wnt and TGF-β signaling are required for the induction of an in vitro model of primitive streak formation using embryonic stem cells. *Proc. Natl Acad. Sci. USA* **103**, 16806–16811 (2006).
30. Séguin, C. A., Draper, J. S., Nagy, A. & Rossant, J. Establishment of endoderm progenitors by SOX transcription factor expression in human embryonic stem cells. *Cell Stem Cell* **3**, 182–195 (2008).

METHODS

Ethics statement. The embryonic-like sacs lack the primitive endoderm and the trophoblast, and thus cannot form yolk sac and placenta, respectively. Therefore, these embryonic-like tissues do not have human organismal form or potential. Furthermore, all experiments were terminated by no later than day 4 in vitro. All protocols used in this work with hPSCs to model early post-implantation human embryo development, including the development of embryonic-like sacs and specifications of hPGCLCs and primitive streak-like cells, have been approved by the Human Pluripotent Stem Cell Research Oversight Committee at the University of Michigan, Ann Arbor.

Cell lines. hPSC lines used in this study include H1 human ES cell (WA01, WiCell; NIH registration number: 0043), H9 human ES cell (WA09, WiCell; NIH registration number: 0062) and 1196a (a human iPSC line from the University of Michigan Pluripotent Stem Cell Core[31]). All hPSC lines have been authenticated by original sources as well as in-house by immunostaining for pluripotency markers and successful differentiation to the three germ layers. All hPSC lines are maintained in a feeder-free system for at least ten passages and authenticated as karyotypically normal. Karyotype analysis was performed by Cell Line Genetics. All hPSC lines are tested negative for mycoplasma contamination (LookOut Mycoplasma PCR Detection Kit, Sigma-Aldrich).

Cell culture. hPSCs were maintained in a standard feeder-free culture system using mTeSR medium (mTeSR; STEMCELL Technologies) or TeSR-E8 medium (Essential 8 or E8; STEMCELL Technologies) and lactate dehydrogenase-elevating virus (LDEV)-free, human ES cell-qualified reduced growth factor basement membrane matrix Geltrex (Thermo Fisher Scientific; derived from Engelbreth-Holm-Swarm tumours similarly to Matrigel). Cell cultures were visually examined during each passage to ensure absence of spontaneously differentiated, mesenchymal-like cells in culture. All hPSCs were used before reaching P70.

Device fabrication. The microfluidic device consists of a polydimethylsiloxane (PDMS) structure layer bonded to a coverslip. The PDMS structure layer is made by mixing PDMS curing agent and base polymer (Sylgard 184; Dow Corning) at a ratio of 1:10 before casting PDMS prepolymer onto a microfabricated silicon mould and baking at 110 °C for 40 min. Medium reservoirs (8 mm in diameter) and gel-loading ports (1.2 mm in diameter) were then punched into the PDMS structure layer using Harris Uni-Core punch tools (Ted Pella). After cleaning with ethanol and air plasma activation, the PDMS structure layer was bonded to a coverslip before baking at 80 °C overnight. Before usage, the microfluidic device was sterilized under UV light for 30 min. Geltrex diluted in mTeSR (8 mg ml^{-1}) was then injected into the central gel channel and allowed to cure for 10 min at 37 °C in an incubator. The central gel channel was separated from the cell loading and induction channels by trapezoid-shaped supporting posts. Diluted Geltrex matrix was contained in the gel channel by supporting posts owing to surface tension. Upon gelation, Geltrex matrix would contract, generating concave Geltrex pockets between supporting posts. mTeSR medium was immediately added to medium reservoirs to fill both the cell loading and induction channels. The microfluidic device was then incubated at 37 °C and 5% CO_2 for 24 h to stabilize the Geltrex matrix in the gel channel.

Microfluidic assays. Colonies of hPSCs were dissociated by Accutase (Sigma-Aldrich) at 37 °C for 10 min before being suspended in mTeSR as single cells. Cells were then centrifuged and resuspended in mTeSR containing 10 μM Y27632 (Tocris), a ROCK inhibitor that prevents dissociation-induced apoptosis of hPSCs[32], at a concentration of 8×10^6 cells per ml. After aspirating mTeSR from medium reservoirs, 10 μl hPSC suspension was introduced into the cell-loading channel ($t = -18$ h). The microfluidic device was then tilted 90° for 10 min to allow cell settlement into Geltrex pockets and their clustering and adhesion to Geltrex matrix. Medium reservoirs were then refilled with fresh mTeSR medium containing 10 μM Y27632. At $t = 0$ h, all medium reservoirs were switched to a fresh basal medium comprising Essential 6 medium (E6; Thermo Fisher Scientific) and FGF2 (20 ng ml^{-1}; GlobalStem). Unless noted otherwise, all medium reservoirs and both cell loading and induction channels were filled with basal medium from $t = 0$ h onwards and were replenished daily.

To generate epiblast-like cysts, basal medium was used in all medium reservoirs from $t = 0$ h onwards. To examine possible involvements of different signalling events in the development of epiblast-like cysts, IWP2 (5 μM; Tocris), LDN 193189 (0.5 μM; Selleckchem), SB 431542 (10 μM; Cayman Chemical) or caspase 3 inhibitor Z-DEVD-FMK (5–40 μM; BioVision) was supplemented into basal medium.

To generate P-ELS, BMP4 (50 ng ml^{-1}; R&D Systems) was supplemented into basal medium in the induction channel from $t = 0$ h onwards. To generate A-ELS, in addition to BMP4 (50 ng ml^{-1}) supplemented into basal medium in the induction channel, noggin (50 ng ml^{-1}; R&D Systems) and IWP2 (5 μM in DMSO; Tocris) were supplemented into basal medium in the cell-loading channel from $t = 0$ h onwards.

To examine the effect of exogenous Wnt or activin on generating asymmetric embryonic-like sacs, WNT3A (50 ng ml^{-1}; R&D Systems), activin A (50 ng ml^{-1}; R&D Systems) and/or BMP4 (50 ng ml^{-1}) were supplemented into basal medium in the induction channel.

To examine the development of posterior primitive streak-like cells, from $t = 0$ h onwards, BMP4 (50 ng ml^{-1}) was supplemented into basal medium in the cell-loading channel, and basal medium or basal medium supplemented with IWP2 (5 μM), IWR1 (10 μM; Selleckchem and STEMCELL Technologies), or noggin (50 ng ml^{-1}) was loaded into the induction channel. To examine anterior primitive streak-like cell development, in addition to BMP4 (50 ng ml^{-1}) supplemented into basal medium in the cell-loading channel, activin A (50 ng ml^{-1}) was added into basal medium in the induction channel.

A detailed protocol describing the implementation of the microfluidic device for generating epiblast-like cysts, P-ELS and A-ELS from hPSCs is available from Protocol Exchange[33].

Immunocytochemistry. hPSCs were fixed in 4% paraformaldehyde (PFA; buffered in 1X PBS) for 12 h, and permeabilized in 0.1% SDS solution (sodium dodecyl sulphate, dissolved in PBS) for another 3 h. Samples were then blocked in 4% donkey serum (Sigma-Aldrich) at 4 °C for 24 h, followed by incubation with primary antibody solutions at 4 °C for another 24 h. Samples were then labelled with donkey -raised secondary antibodies (1:500 dilution) at 4 °C for 24 h. 4′,6-diamidino -2-phenylindole (DAPI; Thermo Fisher Scientific) was used for counterstaining cell nuclei. Alexa Fluor dye-conjugated WGA (Thermo Fisher Scientific) and phalloidin (Invitrogen) were used for visualization of cell membrane and actin microfilaments, respectively. Both primary and secondary antibodies were prepared in 4% donkey serum supplemented with 0.1% NaN_3. Seventy microlitre antibody solutions were added to each medium reservoir for immunostaining. All primary antibodies used in this study are listed in Supplementary Table 2.

The asymmetric embryonic-like sac structure was assessed by immunocytochemistry to confirm molecular asymmetry at $t = 36$ h (for P-ELS: co-staining for TFAP2A and T; for A-ELS: co-staining for TFAP2A and NANOG).

In situ hybridization. In situ hybridization was performed using the ViewRNA ISH Tissue Assay Kit (1-plex; Thermo Fisher Scientific) according to the manufacturer's instructions. In brief, cystic tissues within the microfluidic device were fixed with 4% PFA for 24 h, before being dehydrated by washing with PBT (0.1% Triton X-100 in PBS) and then a graded series of methanol (25%, 50%, 75% and 100% in PBT; twice in each concentration and 10 min for each wash). Before hybridization, cystic tissues were rehydrated using a reverse-graded series of methanol (75%, 50% and 25% in PBT) before being washed twice with PBS. Proteinase K digestion was conducted for 15 min at 40 °C, followed by 4% PFA fixation for 15 min at room temperature. Cystic tissues were hybridized with ViewRNA type 1 probe set for 3 h at 40 °C, followed by treatment with PreAmplifier for 30 min at 40 °C, Amplifier for 20 min at 40 °C, label probe-AP for 20 min at 40 °C, AP-enhancer for 8 min at room temperature, and Fast Red for 35 min at 40 °C. Gene-specific probes for human *AXIN2* (VA1-10388-VT) and *BMP4* (VA1-18826-VT) were tested in this work. Probes against human *ACTB* (VA1-10351-VT) and *Bacillus subtilis dapB* (VF1-11712-VT) were used as positive and negative controls, respectively.

Microscopy. All confocal micrographs were acquired using an Olympus DSUIX81 spinning-disc confocal microscope equipped with an EMCCD camera (iXon X3, Andor). For 3D reconstruction, *z*-stack images were acquired with a slice thickness of 1 μm. Low-magnification bright-field images were acquired using a Labomed TCM 400 inverted microscope equipped with an UCMOS eyepiece camera (Fisher Scientific). For morphogenetic quantification, bright-field or phase-contrast images were acquired using a Zeiss Observer.Z1 microscope (Carl Zeiss MicroImaging) equipped with a monochrome CCD camera (AxioCam, Carl Zeiss MicroImaging). Live imaging was conducted using the Zeiss Observer.Z1 microscope enclosed in an environmental incubator (XL S1 incubator, Carl Zeiss MicroImaging) maintaining cell culture at 37 °C and 5% CO_2.

Enumeration of total cell number. For enumeration of cell number during the development of lumenal cystic tissues, a CAG-H2B-eGFP H9 human ES cell line was generated. H2B-eGFP (Addgene plasmid 32610) was PCR amplified, and the PCR product was ligated into the ePiggyBac vector with a constitutively active puromycin selection cassette[34]. The plasmid was co-transfected with pCAG-PBase (ePiggyBac transposase helper plasmid, a gift from A. H. Brivanlou) using GeneJammer (Agilent Technologies) into H9 human ES cells that were plated at 50,000 cells per cm^2 24 h before transfection. Puromycin selection (2 μg ml^{-1}) started at day 2 after transfection for 4 days. The brightest human ES cell clone was hand-picked and expanded before cell enumeration assays. Cell number of lumenal cystic tissues was manually counted by blinded observers using 3D reconstructed *z*-stack images recorded by confocal microscopy at $t = 0$ h, 24 h and 36 h under different microfluidic experimental conditions.

Morphogenetic quantification. Morphogenetic quantifications, including equivalent cyst diameter, embedded cyst perimeter percentage and amniotic ectoderm-like tissue thickness, were performed manually with AxioVision (Carl Zeiss MicroImaging) using bright-field images. Equivalent cyst diameter was calculated as the average of the longest and shortest axis of each cyst. Thickness

of amniotic ectoderm-like tissue was quantified as the thickness of the thinnest amniotic ectoderm-like tissue region. Embedded cyst perimeter percentage was calculated as the ratio between the perimeter of lumenal cyst embedded in Geltrex matrix and the total cyst perimeter.

Enumeration of hPGCLCs. Cells double positive for TFAP2C and SOX17 ($TFAP2C^+SOX17^+$) were identified as hPGCLCs[21,24,25]. The amniotic ectoderm-like compartment was first identified as the flattened, single-cell layer tissue at $t = 28$, 30 and 36 h or the part of embryonic-like sacs between supporting posts at $t = 24$ h directly exposed to BMP4 stimulation. The amniotic ectoderm-like compartment was then divided into four quadrants. The two middle quadrants furthest away from the epiblast-like pole were defined as the central amniotic ectoderm-like region (CEN-AM). The two quadrants at the junction of epiblast-like and amniotic ectoderm-like compartments were defined as the epiblast-amniotic ectoderm region (EPI-AM). For consistency, only confocal images recorded at the central focal plane of each cyst (40 μm above the microfluidic device bottom surface) were used for enumeration of hPGCLCs. Confocal images were analysed manually by blinded observers using ImageJ to determine the numbers of single ($TFAP2C^+$ or $SOX17^+$), double ($TFAP2C^+SOX17^+$) and triple ($TFAP2C^+NANOG^+SOX17^+$) positive cells in different compartments of embryonic-like sacs.

Transwell assays. Transwell assays were conducted using 12-mm Transwells with porous polyester membrane inserts (0.4 μm pore size; Corning). The Transwell membrane insert was first incubated with 1% Geltrex diluted in DMEM/F12 (Thermo Fisher Scientific) for 1 h. hPSCs suspended in mTeSR containing 10 μM Y27632 were then seeded onto the membrane insert at a density of 3×10^4 cells per cm^2. Eighteen hours after cell seeding, culture medium was switched to basal medium supplemented with or without BMP4 (50 ng ml^{-1}), and cells were cultured for another 48 h. At this point, culture medium was replaced with fresh basal medium before small clusters of undifferentiated hPSCs suspended in basal medium were plated onto the transwell membrane insert or the lower dish. Cells were cultured for another 48 h in basal medium with or without IWP2 (5 μM, dissolved in DMSO) before analysis.

Quantification of T. The epiblast-like compartment of P-ELS was divided into four quadrants, on the basis of their relative distance to the amniotic ectoderm-like pole. Nuclear intensity of T was determined for individual cells in each quadrant by manually selecting a small area in the cell nucleus and measuring the average fluorescence intensity using ImageJ. Care was taken to ensure that selected nuclear areas did not overlap with other nuclei. T intensity for each cell was further normalized to DAPI intensity in the same nuclear area. An average normalized T intensity for cells in each quadrant was then calculated. T intensity of each quadrant was then normalized again to the quadrant with the highest T intensity and plotted.

Signalling reporter lines. A H9 human ES cell line expressing a C-terminal fusion of the T gene with mNeonGreen was generated by CRISPR–Cas9 facilitated homology directed repair (HDR). In brief, activity of guide RNAs (gRNAs) was first screened in HEK 293T cells. An active gRNA with the targeting sequence gccttgctgcttcacatgga, which showed the best activity, was selected and cloned into a second modified version of px330[35]. For the targeting construct, approximately 1,000 bp upstream and downstream of the CRISPR–Cas9 cleavage site and T stop codon was prepared by long PCR and cloned into pBluescript II KS+ (Stratagene), which was modified by adding OriP. This targeting construct was further modified by silent mutation of the gRNA targeting sequence, removal of the natural T stop codon and insertion of a 22 amino acid glycine–serine–alanine-rich flexible linker N-terminal to mNeonGreen, in frame with the T coding sequence.

To generate TCF/Lef reporter-human ES cell lines, 6XTCF/Lef-hsp68-H2B-eGFP was first amplified from a plasmid provided by A.-K. Hadjantonakis (Addgene plasmid no. 32610). The amplified PCR product was ligated into an ePiggyBac vector with a constitutively active puromycin selection cassette[34]. Transfection and puromycin selection were conducted as for construction of the CAG-H2B-eGFP cell line described above. Ten clonal lines were hand-picked and further expanded. H2B–eGFP expression was confirmed by fluorescence microscopy with treatment with CHIR99021 (8 μM; Cayman Chemical) and bFGF (20 ng ml^{-1}) in E6 medium. Two clonal lines with the highest and most homogeneous fluorescence signal were selected for live imaging.

Fluorescence intensity map. Heat maps of fluorescence micrographs were generated using the matplotlib package in Python. Image masks were first generated by thresholding images of DAPI staining and isolating nuclear areas from the background. Immunostaining images were then converted to heat maps on the basis of their fluorescence intensity.

Dextran diffusion assay. Morphogen diffusion in the microfluidic device was determined using fluorescein-labelled dextran (70 kDa, Invitrogen). In brief, 10 μM fluorescein-labelled dextran was supplemented into the induction channel from $t = 30$ h onwards during the development of P-ELS. Fluorescence intensities within the cell loading channel and induction channel were then measured using confocal microscopy at $t = 36$ h.

scRNA-seq and data analysis. P-ELS at $t = 48$ h were treated with Accutase for 1 h to obtain single-cell suspensions. Cells from six microfluidic devices were collected and pooled into PBS containing 0.5% BSA. Transwell-AMLCs were obtained by treating human ES cells with BMP4 (50 ng ml^{-1}) for 48 h using the Transwell method. Transwell-AMLCs were treated with Accutase for 1 h to obtain single-cell suspensions. human ES cells maintained on standard tissue culture plates were dissociated into single cells using Accutase for 1 h. Transwell-AMLCs and human ES cells were counted before being mixed at a 2:1 ratio as a single-cell suspension. Within 1 h after cell dissociation, cells were loaded into the 10x Genomics Chromium system. 10x Genomics v.2 libraries were prepared according to the manufacturer's instructions. Libraries were then sequenced with a minimum coverage of 50,000 raw reads per cell on an Illumina HiSeq 4000 with paired-end sequencing. scRNA-seq data were aligned and quantified using Cell Ranger Single-Cell Software Suite (v.3.0.0, 10x Genomics) against the hg19 human reference genome.

Merging of scRNA-seq data and cell clustering was performed using the Seurat R package (v.3.0.0.9)[36,37]. Default setups were used unless noted otherwise. In brief, cells with nfeature_RNA $\leq$ 3,200 or $\geq$ 6,200 (P-ELS), nfeature_RNA $\leq$ 3,600 or $\geq$ 6,400 (Transwell-AMLC and human ES cell), or cells in which the total mitochondrial gene expression exceeded 6% of total gene expression were discarded from analysis. Gene expression was calculated by normalizing the raw count by the total count before being multiplied by 10,000 and log-transformed. After cell-cycle regression, principal component analysis was performed using the RunPCA function in Seurat. Identification of cell clusters by a shared nearest neighbour (SNN) modularity optimization based clustering algorithm was achieved using the FindClusters function with a resolution set at 0.3. Dimensionality reduction using *t*- SNE was generated using RunTSNE (dim = 1:15).

Differentially expressed genes (DEGs) were identified using FindAllMarkers, with a minimal fold difference of 0.25 in the logarithmic scale and >25% detection rate in either of the two cell types under comparison. Violin plots were generated using VlnPlot in the Seurat R package. Heat maps were plotted on the basis of relative expression (*Z*-score) of top-20 gene signatures to distinguish each cell cluster. GO analyses were performed using DAVID Bioinformatics Resources 6.8 on the basis of DEGs (Supplementary Table 1). For comparison with published data, gene expression data obtained from different platforms (GEO repository, NCBI) were first transformed into $\log_2$(reads per million mapped reads (RPM) + 1). Average expression level of each cell type was used for calculation of correlation coefficient and heat map plotting.

Reporting Summary. Further information on research design is available in the Nature Research Reporting Summary linked to this paper.

Data availability

Data supporting the findings of this study are available within the article and its Supplementary Information files and from the corresponding author upon request. scRNA-seq data are also available at the Gene Expression Omnibus under accession no. GSE134571. All Source Data for graphs included in the paper are available in the online version of the paper.

Code availability

MATLAB and RStudio scripts used in this work are available from the corresponding author upon request.

31. Villa-Diaz, L. G. et al. Synthetic polymer coatings for long-term growth of human embryonic stem cells. *Nat. Biotechnol.* **28**, 581–583 (2010).
32. Watanabe, K. et al. A ROCK inhibitor permits survival of dissociated human embryonic stem cells. *Nat. Biotechnol.* **25**, 681–686 (2007).
33. Zheng, Y. & Fu, J. Protocol for controlled modeling of human epiblast and amnion development using stem cells. *Protoc. Exch.* https://doi.org/10.21203/rs.2.11520/v1 (2019).
34. Lacoste, A., Berenshteyn, F. & Brivanlou, A. H. An efficient and reversible transposable system for gene delivery and lineage-specific differentiation in human embryonic stem cells. *Cell Stem Cell* **5**, 332–342 (2009).
35. Cong, L. et al. Multiplex genome engineering using CRISPR/Cas systems. *Science* **339**, 819–823 (2013).
36. Butler, A., Hoffman, P., Smibert, P., Papalexi, E. & Satija, R. Integrating single-cell transcriptomic data across different conditions, technologies, and species. *Nat. Biotechnol.* **36**, 411–420 (2018).
37. Satija, R., Farrell, J. A., Gennert, D., Schier, A. F. & Regev, A. Spatial reconstruction of single-cell gene expression data. *Nat. Biotechnol.* **33**, 495–502 (2015).

Acknowledgements This work is supported by the University of Michigan Mechanical Engineering Faculty Support Fund (J.F.), the Michigan–Cambridge Research Initiative (J.F.), the University of Michigan Mcubed Fund (J.F.), the National Institutes of Health (R01 DK089933, D.L.G.) and the California Institute for Regenerative Medicine (RB5-07409, V.M.W.). Y.S. was partially supported by the University of Michigan Rackham Predoctoral Fellowship. The Lurie

Nanofabrication Facility at the University of Michigan is acknowledged for support with microfabrication.

Author contributions Y.Z. and J.F. conceived and initiated the project; Y.Z. designed, performed and quantified most experiments, including scRNA-seq data analysis and interpretation; X.X. maintained cell culture, participated in experiments and independently repeated experiments; Y.S. helped to design experiments; S.W. developed the TCF/Lef:H2B-GFP reporter line and helped with scRNA-seq data analysis; Z.L. fabricated silicon moulds; S.N.E. helped with hPGCLC-related experiments; J.M.M., J.N.L. and V.M.W. provided the T-mNeonGreen reporter line; Y.Z., D.L.G. and J.F. wrote the manuscript; J.F. supervised the study. All authors edited and approved the manuscript.

Competing interests Y.Z., Y.S., S.N.E., D.L.G. and J.F. have filed a provisional patent related to this work (United States Provisional Patent Application No. 62/431,907).

Additional information

Supplementary information is available for this paper at https://doi.org/10.1038/s41586-019-1535-2.

Correspondence and requests for materials should be addressed to J.F.

Peer review information *Nature* thanks Nicolas Rivron and the other, anonymous, reviewer(s) for their contribution to the peer review of this work.

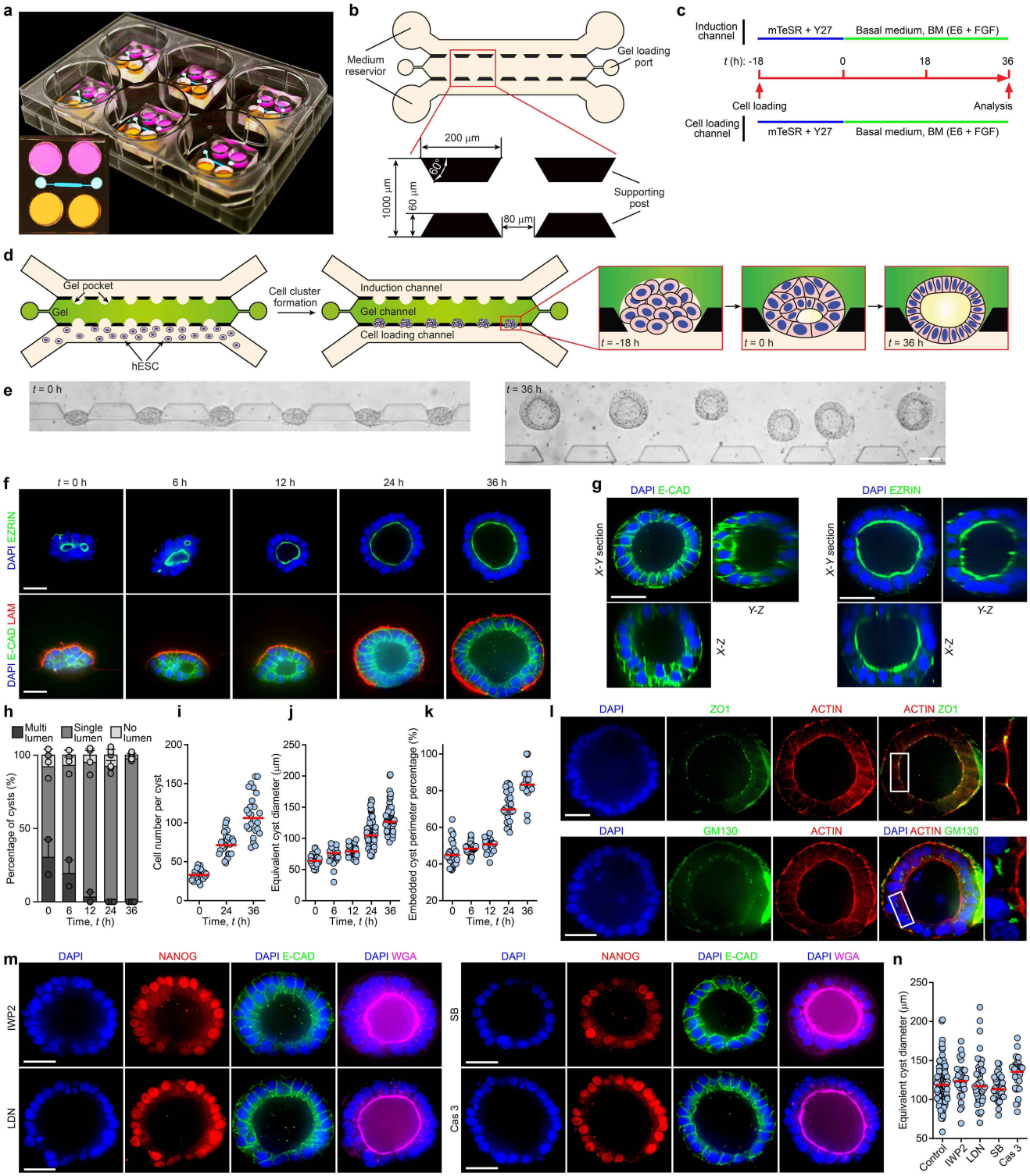

Extended Data Fig. 1 | See next page for caption.

Extended Data Fig. 1 | Microfluidic generation of pluripotent epiblast-like cyst. a, Photograph showing microfluidic devices in a six-well plate. Inset shows a top view of the device. Devices were filled with medium containing food colour dyes to illustrate medium reservoirs and microfluidic channels. **b**, Design of microfluidic device incorporating three parallel channels (80 μm in height) partitioned by trapezoid-shaped supporting posts spaced 80 μm apart. The central channel (gel channel) is preloaded with Geltrex. The other two open channels are used for cell loading (cell-loading channel) and chemical induction (induction channel), respectively. **c**, Protocol for generating epiblast-like cysts. After cell loading (designated as $t = -18$ h), a basal medium comprising Essential 6 medium and FGF2 (20 ng ml^{-1}) is supplied to both the cell-loading and induction channels from $t = 0$ h onwards. **d**, Schematic showing cell loading, cell clustering and lumenogenesis. After injection of Geltrex into the gel channel, Geltrex gelation and contraction leads to formation of evenly spaced concave gel pockets between supporting posts. After loading human ES cells (hESC) into the cell-loading channel, the microfluidic device is tilted 90° to allow cells to settle into gel pockets ($t = -18$ h). At $t = 0$ h, nascent lumenal cavities emerge within cell clusters. At $t = 36$ h, epiblast-like cysts contain a single central lumenal cavity reminiscent of the pro-amniotic cavity formed in the epiblast of the blastocyst upon implantation. **e**, Representative bright-field images showing an array of epiblast-like cysts at $t = 0$ h and 36 h. Experiments were repeated five times with similar results. Scale bar, 80 μm. **f**, Representative confocal micrographs showing epiblast-like cysts at indicated time points stained for ezrin (top) or E-cadherin (E-cad) and laminin (Lam; bottom). Nuclei were stained with DAPI. Some epiblast-like cysts initiate lumenogenesis with multiple small ezrin^{+} lumenal cavities, which gradually resolve into a single central lumen, probably through cavity fusion. Scale bars, 40 μm. Experiments were repeated three times with similar results. **g**, Representative confocal micrographs showing *X*–*Y*, *X*–*Z* and *Y*–*Z* sections of epiblast-like cysts obtained at $t = 36$ h, stained for E-cadherin and ezrin. Nuclei were stained with DAPI. Scale bars, 40 μm. Experiments were repeated twice with similar results. **h**, Percentage of epiblast-like cysts with single, multiple or no lumenal cavities at indicated time points. $n = 59$, 57, 60, 89 and 110 cysts for $t = 0$ h, 6 h, 12 h, 24 h and 36 h, respectively. Data were pooled from $n = 2$ (0 h, 6 h, 12 h) or 3 (24 h and 36 h) independent experiments. Data represent the mean ± s.e.m. **i**, Cell number in each epiblast-like cyst as a function of time. $n = 26$ cysts for each time point. Data were pooled from $n = 2$ independent experiments. Red lines represent the median. **j**, Equivalent epiblast-like cyst diameter as a function of time. $n = 56$, 45, 50, 115 and 88 cysts for $t = 0$ h, 6 h, 12 h, 24 h and 36 h, respectively. Data were pooled from $n = 3$ independent experiments. Red lines represent the median. **k**, Embedded epiblast-like cyst perimeter percentage as a function of time. $n = 33$, 35, 26, 28 and 21 cysts for $t = 0$ h, 6 h, 12 h, 24 h and 36 h, respectively. Data were pooled from $n = 2$ independent experiments. Red lines represent the median. **l**, Representative confocal micrographs showing epiblast-like cysts at $t = 36$ h stained for ZO1 and actin (top) or GM130 and actin (bottom). Nuclei were stained with DAPI. Far right, magnified views of outlined regions. Scale bars, 40 μm. Experiments were repeated twice with similar results. **m**, Representative confocal micrographs showing epiblast-like cysts obtained at $t = 36$ h with indicated drugs supplemented into basal medium from $t = 0$–36 h. IWP2, 5 μM; BMP inhibitor LDN 193189 (LDN), 0.5 μM; TGF-β inhibitor SB 431542 (SB), 10 μM; Caspase 3 inhibitor Z-DEVD-FMK (Cas 3), 10 μM. Cysts were stained for NANOG and E-cadherin. Fluorescently labelled WGA was used to stain plasma membrane. Nuclei were stained with DAPI. Note that assays were also conducted with different concentrations of Z-DEVD-FMK (5 μM, 20 μM and 40 μM), with results compatible with those obtained from 10 μM Z-DEVD-FMK. Scale bars, 40 μm. Experiments were repeated twice with similar results. **n**, Equivalent epiblast-like cyst diameter at $t = 36$ h under indicated conditions. $n = 142$, 37, 44, 40 and 36 cysts for control, IWP2, LDN, SB and Cas 3 conditions, respectively. Data were pooled from $n = 2$ independent experiments. Red lines represent the median.

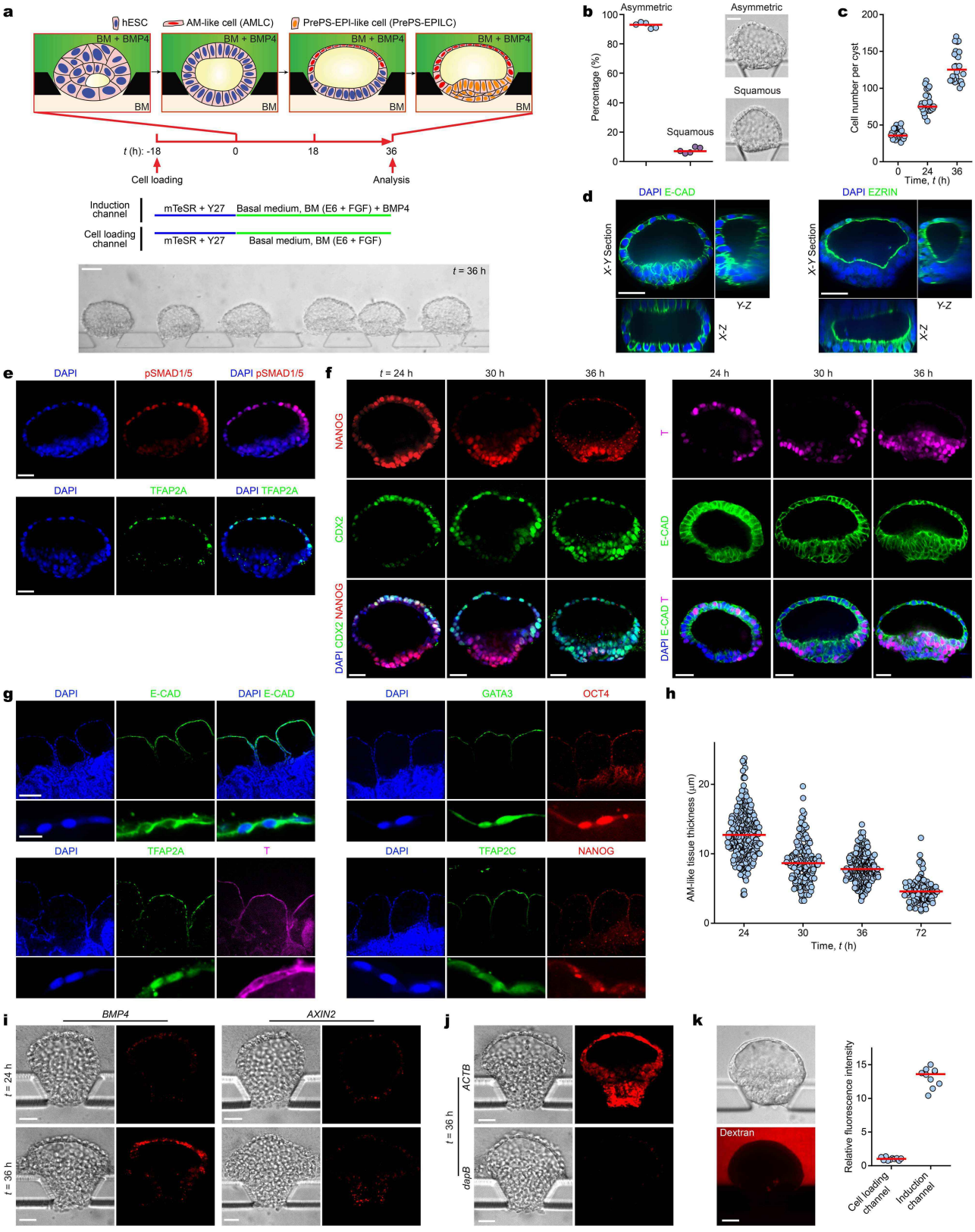

Extended Data Fig. 2 | See next page for caption.

Extended Data Fig. 2 | Progressive development of posteriorized embryonic-like sac. a, Protocol for generating P-ELS. After initial seeding and clustering of human ES cells ($t = -18$ to 0 h), lumenogenesis leads to the formation of the epiblast-like cyst containing a single central lumen. BMP4 stimulation (50 ng ml^{-1}) from the induction channel from $t = 0$ h onwards leads to patterning of the epiblast-like cyst and formation of the asymmetric embryonic-like sac, with specification of the amniotic ectoderm-like fate to cells directly exposed to BMP4 induction. Development of the P-ELS triggers the onset of gastrulation-like events and expression of T in the epiblast-like compartment of the P-ELS. Bright-field image shows an array of P-ELS at $t = 36$ h. Scale bar, 80 μm. Experiments were repeated five times with similar results. **b**, Percentage of P-ELS and uniformly squamous amniotic ectoderm-like cysts at $t = 36$ h. Representative phase-contrast micrographs are shown. Scale bar, 40 μm. $n = 396$ cysts from $n = 5$ independent experiments. Each dot represents data obtained from an independent experiment. Red lines represent the median. **c**, Cell number in each cyst as a function of time. $n = 26$ cysts for each time point. Data were pooled from $n = 2$ independent experiments. Red lines represent the median. **d**, Representative confocal micrographs showing *X*–*Y*, *X*–*Z* and *Y*–*Z* sections of P-ELS at $t = 36$ h stained for E-cadherin and ezrin. Nuclei were stained with DAPI. Scale bars, 40 μm. Experiments were repeated twice with similar results. **e**, Representative confocal micrographs showing P-ELS at $t = 36$ h stained for pSMAD1/5 and TFAP2A. Nuclei were stained with DAPI. Scale bars, 40 μm. Experiments were repeated three times with similar results. **f**, Representative confocal micrographs showing P-ELS at indicated time points co-stained for NANOG and CDX2 (left) or T and E-cadherin (right). Nuclei were stained with DAPI. Scale bars, 40 μm. Experiments were repeated three times with similar results. **g**, Representative confocal micrographs showing amniotic ectoderm-like tissues at $t = 72$ h stained for E-cadherin, GATA3 and OCT4, TFAP2A and T, or TFAP2C and NANOG as indicated. Bottom images show magnified views of amniotic ectoderm-like tissues. Nuclei were stained with DAPI. Scale bars, 40 μm (small panels) and 160 μm (large panels). Experiments were repeated five times with similar results. **h**, Thickness of amniotic ectoderm-like tissue as a function of time. $n = 267$, 167, 258 and 111 cysts for $t = 24$ h, 30 h, 36 h and 72 h, respectively. Data were pooled from $n = 5$ independent experiments. Red lines represent the median. **i**, In situ hybridization images of P-ELS at $t = 24$ h and $t = 36$ h for *BMP4* (left) and *AXIN2* (right). Scale bars, 40 μm. Experiments were repeated twice with similar results. **j**, In situ hybridization images of P-ELS at $t = 36$ h for *ACTB* (top) and *B. subtilis dapB* (bottom). Scale bars, 40 μm. Experiments were repeated twice with similar results. **k**, Left, bright-field and fluorescent micrographs showing P-ELS at $t = 36$ h blocking diffusion of fluorescein-labelled dextran (70 kDa) into the cell loading channel. Dextran was supplemented into the induction channel and diffused into the gel channel. Experiments were repeated twice with similar results. Scale bar, 40 μm. Right, plot showing relative fluorescence intensity within the cell-loading channel and induction channel. Data are normalized to the average intensity in the cell loading channel. Our characterization of dextran diffusion shows that the supporting posts and in-between expanding P-ELS effectively block morphogen diffusion across the tissues. $n = 10$ cysts. Data were pooled from $n = 2$ independent experiments. Red lines represent the median.

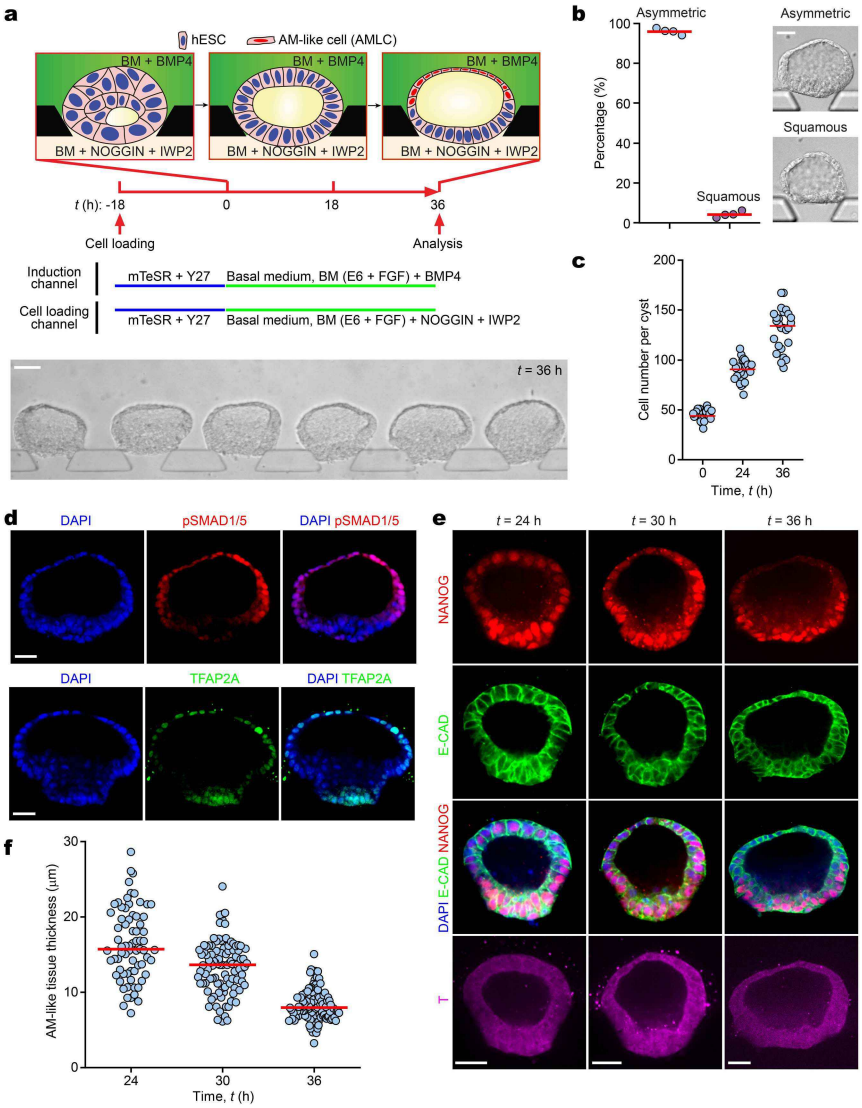

Extended Data Fig. 3 | Progressive development of anteriorized embryonic-like sac. a, Protocol for generating A-ELS. BMP4 (50 ng ml^{-1}) stimulation from the induction channel leads to patterning of the epiblast-like cyst; cells directly exposed to BMP4 are specified to the amniotic ectoderm-like fate. Inhibition of BMP and Wnt signalling by adding noggin (50 ng ml^{-1}) and IWP2 (5 μM) in the cell–loading channel prevents the epiblast-like compartment from losing pluripotency and initiating gastrulation-like events. Bright-field image shows an array of A-ELS at $t = 36$ h. Scale bar, 80 μm. Experiments were repeated three times with similar results. **b**, Percentage of A-ELS and uniformly squamous amniotic ectoderm-like cysts at $t = 36$ h. Representative phase-contrast micrographs are shown. Scale bar, 40 μm. $n = 212$ cysts from $n = 4$ independent experiments. Each dot represents data obtained from an independent experiment. Red lines represent the median. **c**, Cell number in each cyst as a function of time. $n = 26$ cysts for each time point. Data were pooled from $n = 2$ independent experiments. Red lines represent the median. **d**, Representative confocal micrographs showing A-ELS at $t = 36$ h stained for pSMAD1/5 or TFAP2A. Nuclei were stained with DAPI. Scale bars, 40 μm. Experiments were repeated three times with similar results. **e**, Representative confocal micrographs showing A-ELS at indicated time points stained for NANOG, E-cadherin and T. Nuclei were stained with DAPI. Scale bars, 40 μm. Experiments were repeated three times with similar results. **f**, Thickness of amniotic ectoderm-like tissue in A-ELS as a function of time. $n = 71$, 100 and 106 cysts for $t = 24$ h, 30 h and 36 h, respectively. Data were pooled from $n = 3$ independent experiments. Red lines represent the median.

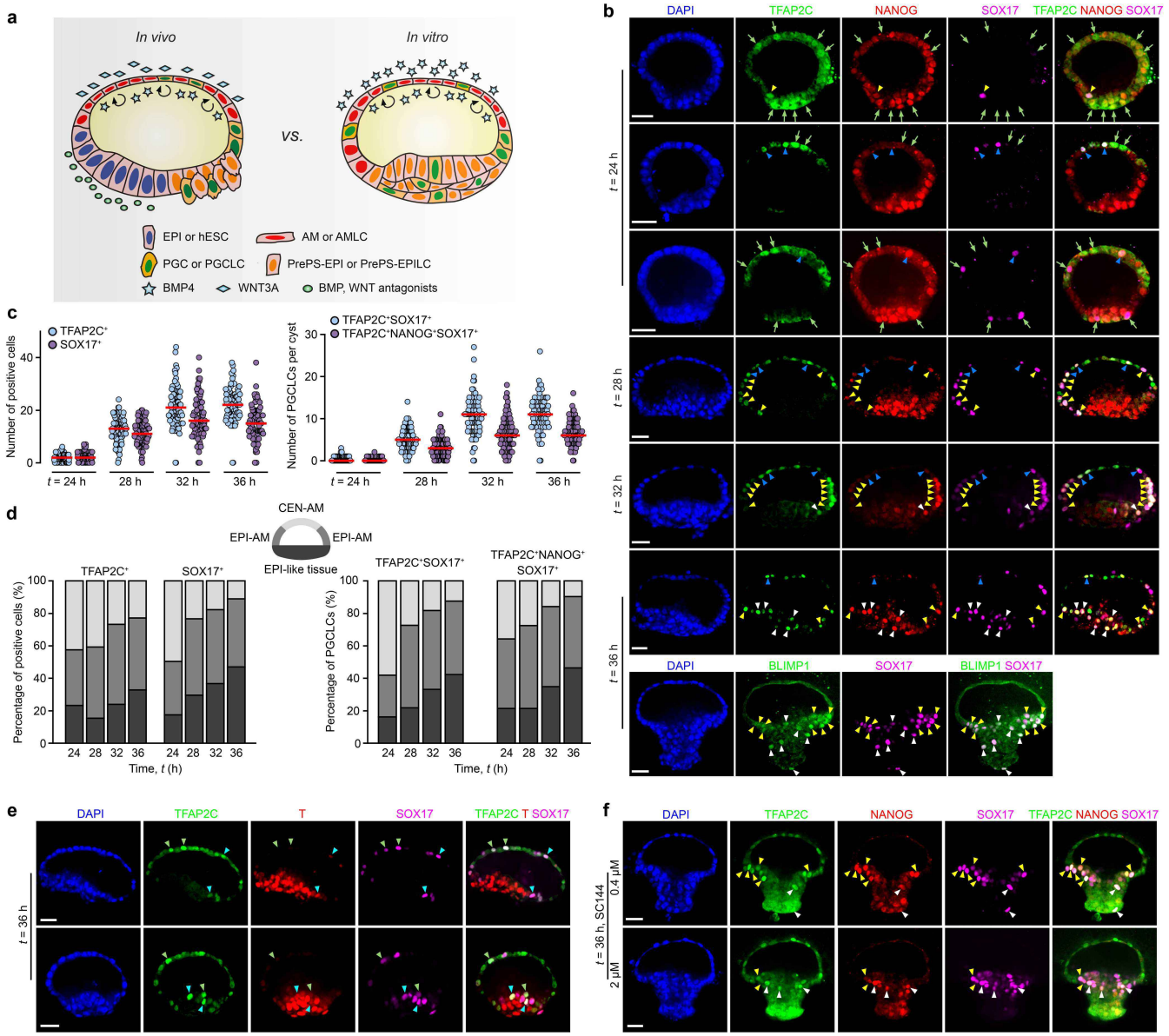

Extended Data Fig. 4 | Specification of human primordial germ cell-like cells in posteriorized embryonic-like sac. a, Specification of PGCs or PGCLCs in the *M. fascicularis* embryo (left; ref. [21]) and P-ELS (right). **b**, Representative confocal micrographs showing P-ELS stained for TFAP2C, NANOG and SOX17 or BLIMP1 and SOX17 at indicated time points. Nuclei were stained with DAPI. TFAP2C$^+$SOX17$^-$ and SOX17$^+$TFAP2C$^-$ cells are marked by green arrows. TFAP2C$^+$SOX17$^+$ cells are identified as nascent, early-stage hPGCLCs. The amniotic ectoderm-like tissue is divided into four quadrants: two middle quadrants furthest away from the epiblast-like pole as central amniotic ectoderm-like compartment (CEN-AM), and two quadrants at the junction of epiblast-like and amniotic ectoderm-like compartments (EPI-AM). TFAP2C$^+$SOX17$^+$ hPGCLCs in the CEN-AM, EPI-AM and epiblast-like compartments are marked by blue, yellow and white arrowheads, respectively. Scale bars, 40 μm. Experiments were repeated three times with similar results. **c**, Left, dot plot of the numbers of TFAP2C$^+$ and SOX17$^+$ cells at indicated time points. Right, dot plot of the numbers of TFAP2C$^+$SOX17$^+$ and TFAP2C$^+$ NANOG$^+$SOX17$^+$ hPGCLCs at indicated time points. $n = 85$, 92, 82 and 80 cysts for $t = 24$ h, 28 h, 32 h and 36 h, respectively. Data were pooled from $n = 3$ independent experiments. Red lines represent the median. **d**, Left, spatial distribution of TFAP2C$^+$ and SOX17$^+$ cells at indicated time points. Right, spatial distribution of TFAP2C$^+$SOX17$^+$ and TFAP2C$^+$NANOG$^+$SOX17$^+$ hPGCLCs at indicated time points. $n = 85$, 92, 82 and 80 cysts for $t = 24$ h, 28 h, 32 h and 36 h, respectively. Data were pooled from $n = 3$ independent experiments. **e**, Representative confocal micrographs showing P-ELS at $t = 36$ h stained for TFAP2C, T and SOX17. Nuclei were stained with DAPI. T-expressing (TFAP2C$^+$SOX17$^+$T$^+$) and T-non-expressing (TFAP2C$^+$SOX17$^+$T$^-$) hPGCLCs are marked by blue and green arrowheads, respectively. Scale bars, 40 μm. Experiments were repeated three times with similar results. **f**, Representative confocal micrographs showing P-ELS treated with different doses of the GP130 inhibitor SC144 (top, 0.4 μM; bottom, 2 μM). P-ELS obtained at $t = 36$ h were stained for TFAP2C, NANOG and SOX17. Nuclei were stained with DAPI. TFAP2C$^+$SOX17$^+$ hPGCLCs in the EPI-AM and epiblast-like compartments are marked by yellow and white arrowheads, respectively. Higher doses of SC144 (8 μM) caused substantial cell death (data not shown). Scale bars, 40 μm. Experiments were repeated twice with similar results.

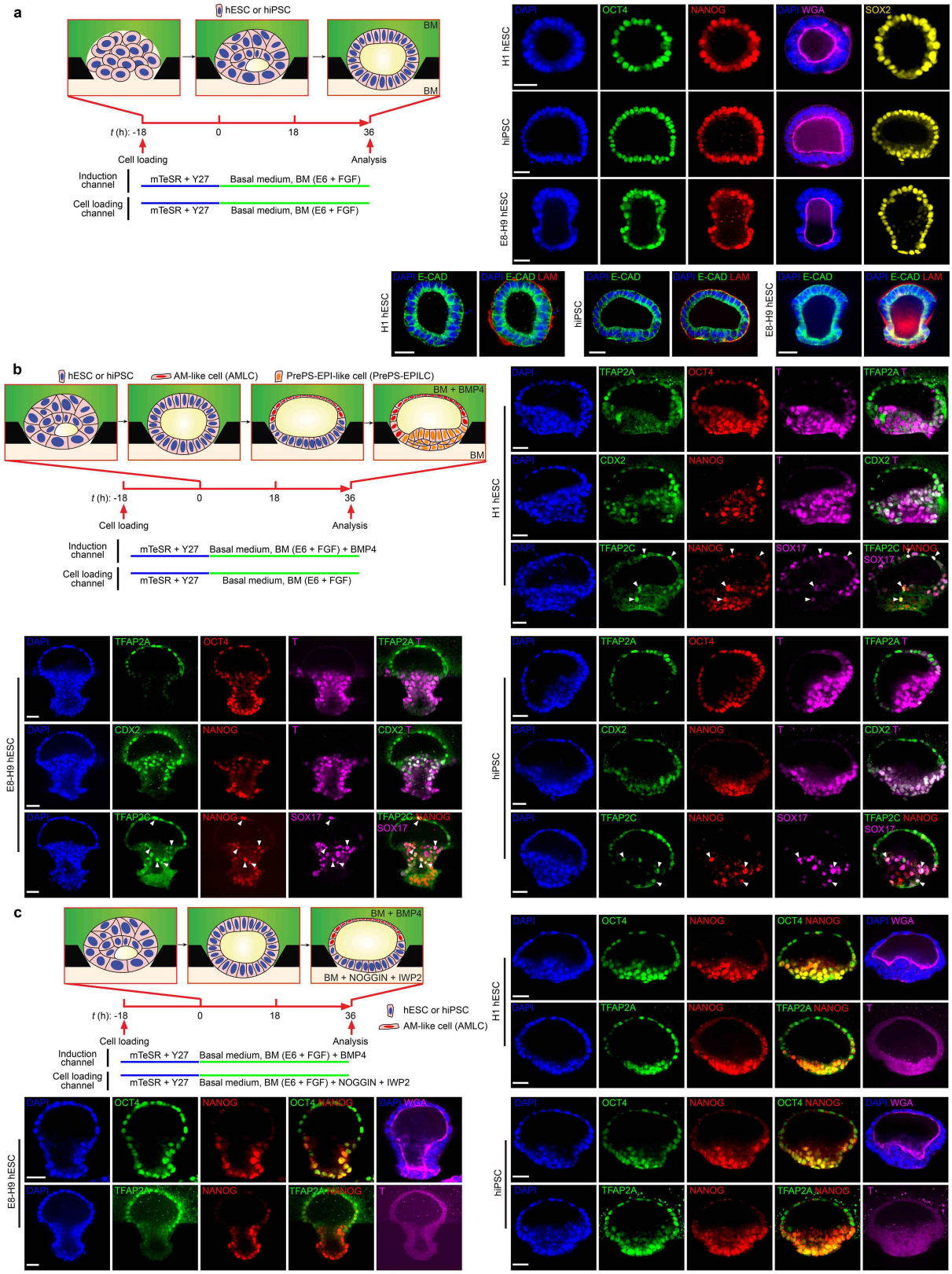

Extended Data Fig. 5 | See next page for caption.

Extended Data Fig. 5 | Microfluidic modelling of human epiblast and amnion development using H1 human ES cells and human induced pluripotent stem cells (hiPSCs) maintained in mTeSR medium as well as H9 human ES cells maintained in Essential 8 medium (E8-H9). a, Microfluidic generation of epiblast-like cysts. The schematic shows culture conditions and cartoons of epiblast-like cyst development. Representative confocal micrographs show epiblast-like cysts generated from H1 human ES cell, hiPSC and E8–H9 human ES cell at $t = 36$ h, stained for OCT4, NANOG, SOX2, E-cadherin and laminin as indicated. Fluorescently labelled WGA was used for staining of plasma membrane. **b**, Microfluidic generation of P-ELS. Schematic shows culture conditions and cartoons of P-ELS development. Representative confocal micrographs show P-ELS generated from H1 human ES cell, hiPSC and E8–H9 human ES cell at $t = 36$ h stained for TFAP2A, OCT4 and T (top); CDX2, NANOG and T (middle); TFAP2C, NANOG and SOX17 (bottom). $TFAP2C^{+}NANOG^{+}SOX17^{+}$ hPGCLCs are marked by white arrowheads. **c**, Microfluidic generation of A-ELS. Culture conditions and cartoons of A-ELS development are shown. Representative confocal micrographs show A-ELS generated from H1 human ES cell, hiPSC and E8–H9 human ES cell at $t = 36$ h stained for OCT4 and NANOG (top); TFAP2A, NANOG and T (bottom). Fluorescently labelled WGA was used for staining of plasma membrane. In **a**–**c**, nuclei were stained with DAPI. Scale bars, 40 μm. All experiments were repeated twice with similar results.

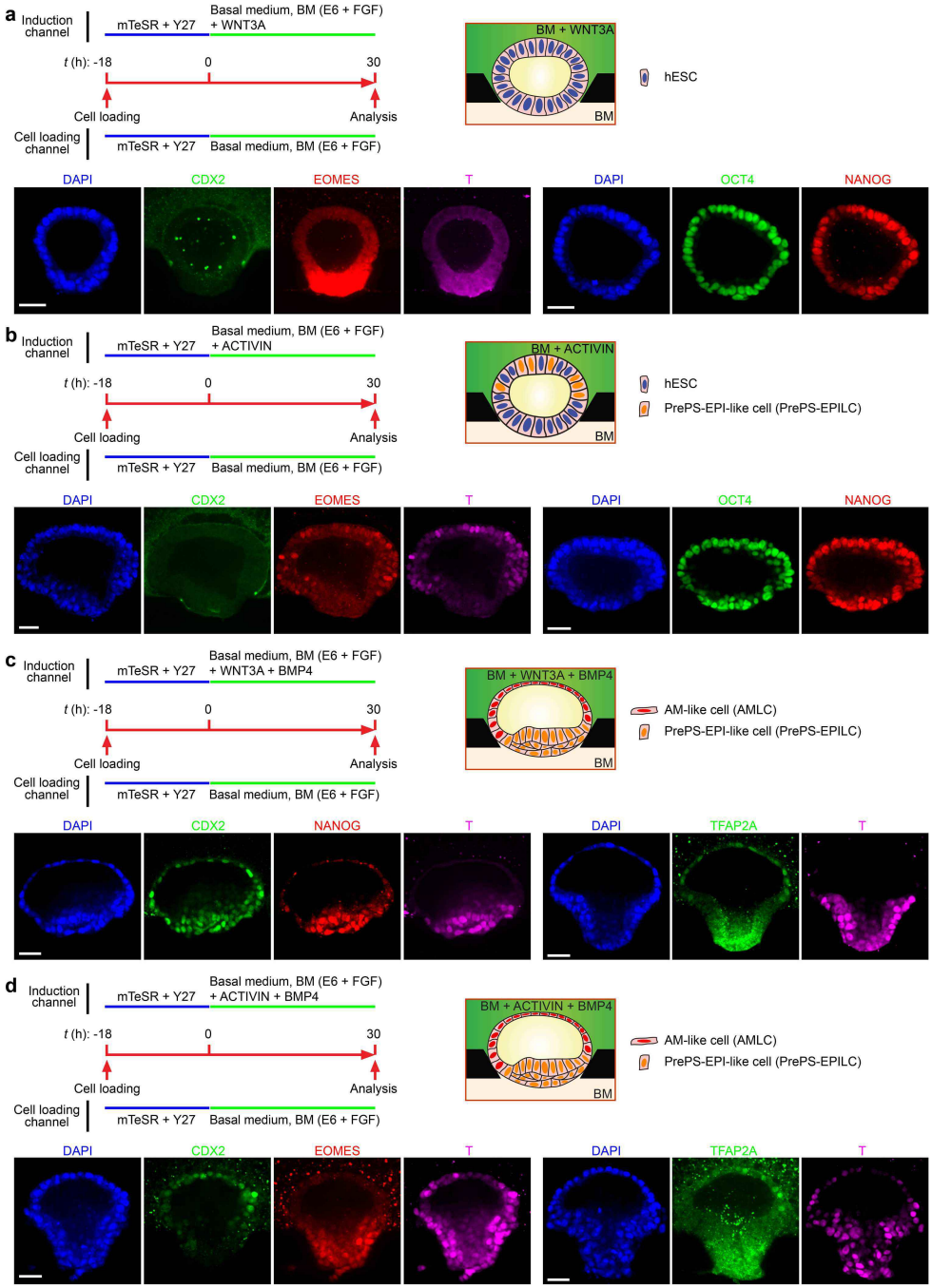

Extended Data Fig. 6 | Exogenous Wnt or activin alone is insufficient to generate asymmetric embryonic-like sacs. Schematics show different culture protocols in which WNT3A (50 ng ml^{-1}), activin A (50 ng ml^{-1}) and/or BMP4 (50 ng ml^{-1}) were supplemented into basal medium in the induction channel as indicated. All cystic tissues were obtained at $t = 30$ h. **a**, Representative confocal micrographs showing cysts stained for CDX2, EOMES and T or OCT4 and NANOG. **b**, Representative confocal micrographs showing cysts stained for CDX2, EOMES and T or OCT4 and NANOG. **c**, Representative confocal micrographs showing cysts stained for CDX2, NANOG and T or TFAP2A and T. **d**, Representative confocal micrographs showing cysts stained for CDX2, EOMES and T or TFAP2A and T. In **a**–**d**, nuclei were stained with DAPI. Scale bars, 40 μm. All experiments were repeated three times with similar results.

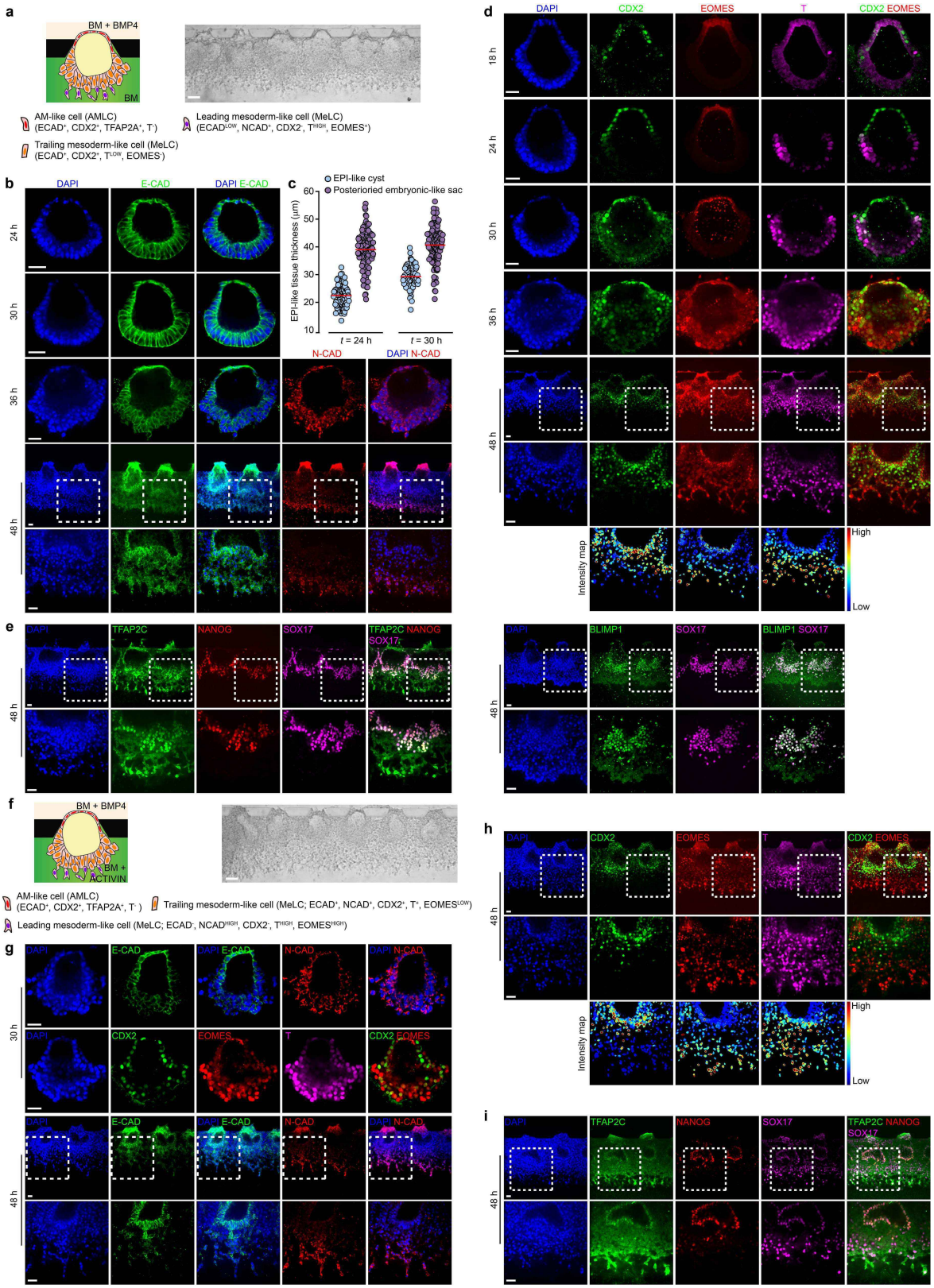

Extended Data Fig. 7 | See next page for caption.

Extended Data Fig. 7 | Molecular characterization of posterior and anterior primitive streak-like cell development. a, Schematic showing posterior primitive streak-like cell development in P-ELS at $t = 48$ h with BMP4 (50 ng ml^{-1}) supplemented into basal medium in the cell-loading channel. Right, bright-field image shows an array of P-ELS at $t = 48$ h. Scale bar, 80 μm. **b**, Representative confocal micrographs show P-ELS stained for E-cadherin and N-cadherin at indicated time points. Thickening of the epiblast-like tissue before the onset of cell dissemination from the PrePS-EPI-like compartment was evident. Outlined regions are magnified in the panel below. **c**, Dot plot of the thickness of the epiblast-like tissue at indicated time points. For $t = 24$ h, $n = 107$ and 116 for epiblast-like cysts and P-ELS, respectively. For $t = 30$ h, $n = 79$ and 135 for epiblast-like cysts and P-ELS, respectively. Data were pooled from $n = 4$ independent experiments. Red lines represent the median. **d**, Representative confocal micrographs showing P-ELS stained for CDX2, EOMES and T at indicated time points. Outlined regions are magnified in the panel below. Intensity maps show relative intensities of corresponding markers as indicated. **e**, Representative confocal micrographs show P-ELS stained for TFAP2C, NANOG and SOX17 (left) or BLIMP1 and SOX17 (right) at $t = 48$ h. Outlined regions are magnified in the panel below. **f**, Schematic showing anterior primitive streak-like cell development in P-ELS at $t = 48$ h with BMP4 (50 ng ml^{-1}) and activin A (50 ng ml^{-1}) supplemented into the cell-loading and induction channels, respectively. Right, bright-field image shows an array of P-ELS at $t = 48$ h. Scale bar, 80 μm. **g**, Representative confocal micrographs showing staining for E-cadherin, N-cadherin, CDX2, EOMES and T at indicated time points. Outlined regions are magnified in the panel below. **h**, Representative confocal micrographs show staining for CDX2, EOMES and T at $t = 48$ h. Outlined regions are magnified in the panel below. Intensity maps show relative intensities of corresponding markers as indicated. **i**, Representative confocal micrographs show staining for TFAP2C, NANOG and SOX17 at $t = 48$ h. Outlined regions are magnified in the panel below. In all immunostaining micrographs, nuclei were stained with DAPI; scale bars, 40 μm. All experiments were repeated twice with similar results.

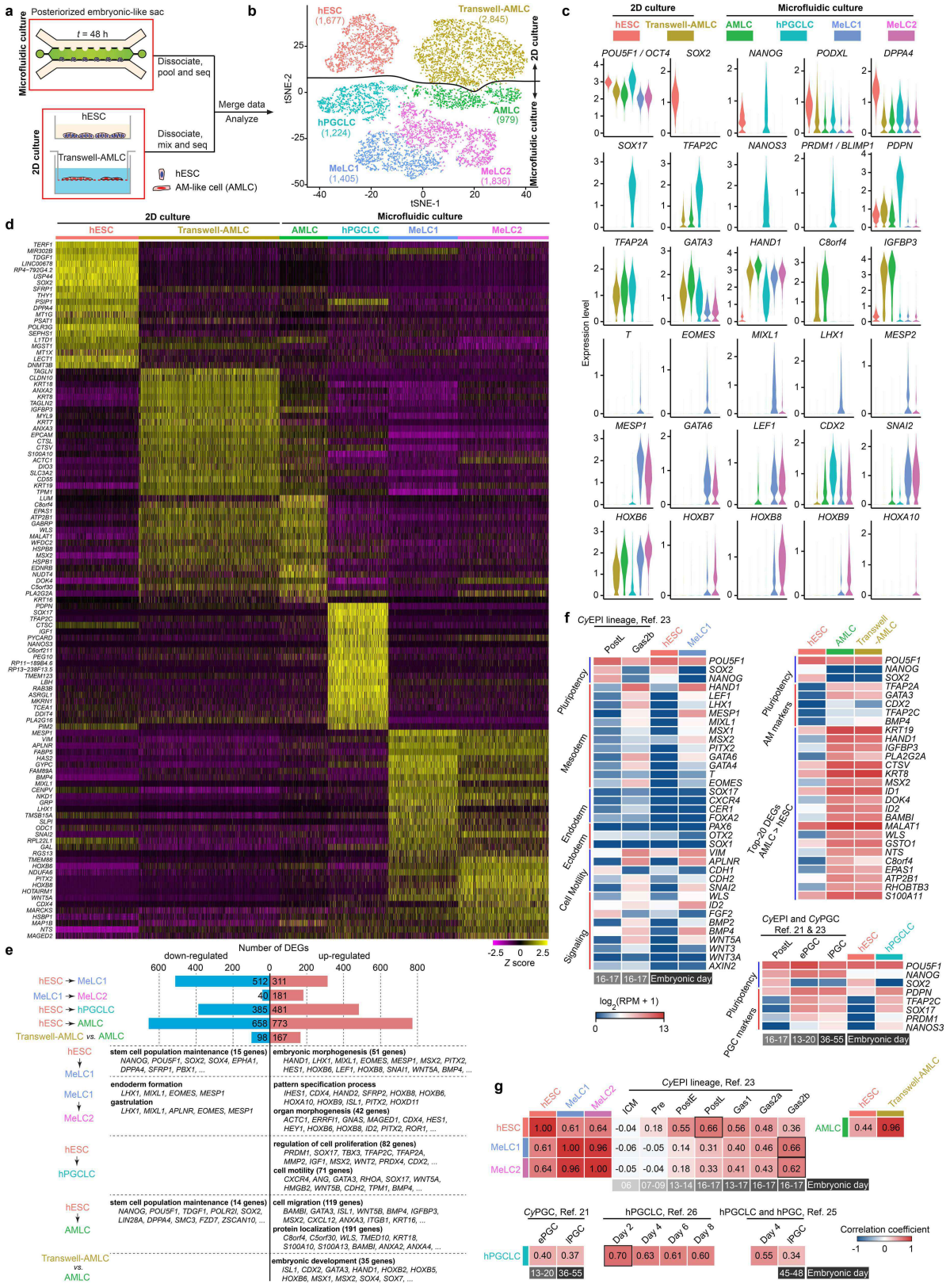

Extended Data Fig. 8 | See next page for caption.

Extended Data Fig. 8 | Cell-type identification and characterization using scRNA-seq. a, Workflow. P-ELS were collected from six microfluidic devices at $t = 48$ h and were dissociated into single cells. AMLCs obtained using the Transwell method (Transwell-AMLC) and human ES cells cultured on tissue culture plates were dissociated into single cells before the cells were mixed at a 1:2 ratio. scRNA-seq was conducted using 10x Genomics and Illumina HiSeq 4000. Single-cell transcriptome data of P-ELS, Transwell-AMLC and human ES cell were merged and analysed. **b**, *t*-SNE plot generated from scRNA-seq data of a total of 9,966 cells, revealing six distinct, colour-coded cell populations (human ES cell, Transwell-AMLC, AMLC, hPGCLC, MeLC1 and MeLC2). Cell numbers of each population are indicated. **c**, Violin plots of log-transformed, normalized expression levels of genes associated with pluripotency (*POU5F1* (also known as *OCT4*), *SOX2*, *NANOG*, *PODXL* and *DPPA4*), hPGC (*SOX17*, *TFAP2C*, *NANOS3*, *BLIMP1* and *PDPN*), amniotic ectoderm (*TFAP2A*, *GATA3*, *HAND1*, *TCIM* (also known as *C8orf4*) and *IGFBP3*), mesoderm (*T*, *EOMES*, *MIXL1*, *LHX1*, *MESP2*, *MESP1*, *GATA6*, *LEF1*, *CDX2* and *SNAI2*) and HOX proteins (*HOXB6*, *HOXB7*, *HOXB8*, *HOXB9* and *HOXA10*) in the six cell populations as indicated. All cells in **b** are used for violin plots. **d**, Heat map of relative expression (*Z*-score) of top-20 gene signatures distinguishing each cell population. **e**, DEGs between different cell clusters (MeLC1 against human ES cell; MeLC2 against MeLC1; hPGCLC against human ES cell; AMLC against human ES cell; AMLC against Transwell-AMLC). Top, red and blue bars indicate the numbers of up- and downregulated DEGs, respectively, in indicated pairwise comparisons. Bottom, enrichment of GO terms and representative genes in DEGs from indicated pairwise comparisons. **f**, Heat map of log-transformed expression levels of selected genes among indicated cell types including those reported by others[21,23]. Genes are grouped on the basis of their associations with embryonic cell fates, cellular functions, developmental signalling or top-20 DEG status. Left, comparisons among *M. fascicularis* epiblast (*Cy*EPI) lineage, human ES cell and MeLC1. Right, comparisons among human ES cell, AMLC and Transwell-AMLC. Top-20 DEGs are identified from those upregulated in AMLC against human ES cell (AMLC > human ES cell). Bottom, comparisons between *Cy*EPI, *Cy*PGC, human ES cell and hPGCLC. **g**, Heat map of correlation coefficients among indicated cell types including those reported by others[21,23,25,26]. Comparisons between human ES cell, MeLC1, MeLC2 and *Cy*EPI lineages are based on ontogenic genes identified for *Cy*EPI (651 in common out of 776)[23]. Comparisons between hPGCLC, *Cy*PGC and hPGC are based on ontogenic *Cy*PGC genes (477 in common out of 544)[21]. Comparisons between human ES cell, Transwell-AMLC and AMLC are based on top-500 DEGs identified in AMLC against human ES cell. Correlation coefficient is calculated using averages of log-transformed expression of common genes. In **f**, **g**, *Cy*EPI lineages: ICM, inner cell mass, E6; Pre, pre-implantation epiblast, E7–E9; PostE and PostL, post-implantation early (E13–E14) and late (E16–E17) epiblast, respectively; Gas1/2a/2b, gastrulating cells, E13–E17. For *Cy*PGC and hPGC: ePGC, early *Cy*PGC, E13–E20; lPGC, late gonadal *Cy*PGC, E36–E55, or late gonadal hPGC, E45–E48. Embryonic days are indicated below the heat maps, and colour bars above and besides the heat maps indicate cell types. All genes are listed in Supplementary Table 1.

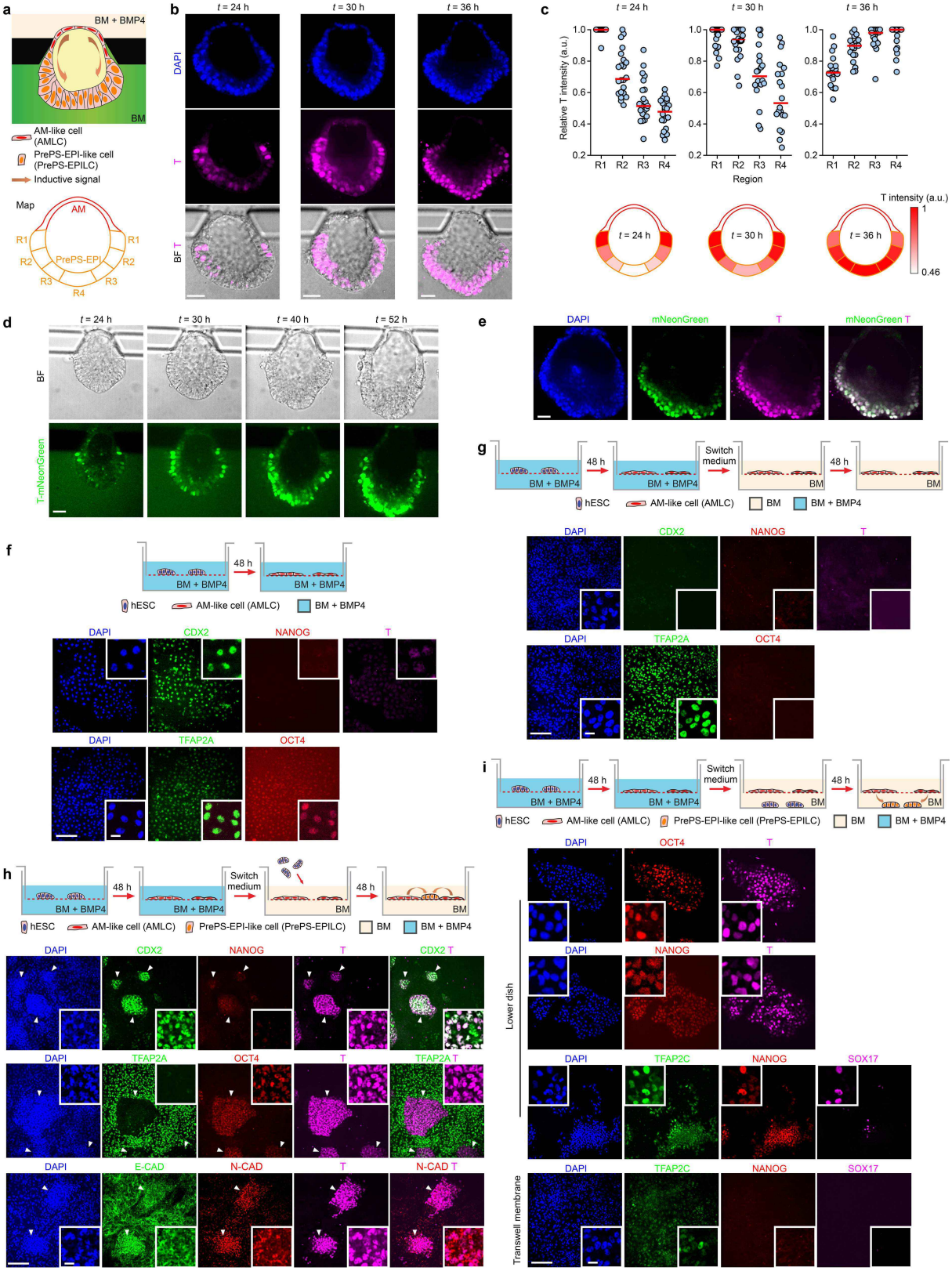

Extended Data Fig. 9 | See next page for caption.

Extended Data Fig. 9 | Inductive effect of amniotic ectoderm-like cells on the onset of gastrulation-like events. a, Schematic showing P-ELS; the PrePS-EPI-like compartment is divided into four quadrants (R1, R2, R3 and R4) for quantification. Basal medium (BM) comprises E6 and FGF2 (20 ng ml^{-1}). BMP4 (50 ng ml^{-1}) was supplemented into the cell-loading channel. **b**, Fluorescent and composite images showing dynamic T expression in the PrePS-EPI-like compartment at indicated time points. Experiments were repeated three times with similar results. **c**, Top, dot plots of relative T intensity in different quadrants of the PrePS-EPI-like compartment at indicated time points. Red lines represent the median. Bottom, spatial maps of average relative T intensity at indicated time points. $n = 22$ (24 h), 20 (30 h) and 20 (36 h) cysts. Data were pooled from $n = 2$ independent experiments. **d**, Live imaging with T-mNeonGreen human ES cell reporter line to track dynamic T expression in the PrePS-EPI-like compartment during the development of P-ELS. **e**, Characterization of T-mNeonGreen human ES cell reporter line showing co-localization of neon green signal and immunostaining of T. **f**, Representative confocal micrographs showing development of AMLCs by culturing human ES cells on Transwell membranes in basal medium supplemented with BMP4 (50 ng ml^{-1}) for 48 h. Cells were stained for CDX2, NANOG and T (top) or TFAP2A and OCT4 (bottom). **g**, Representative confocal micrographs showing AMLCs stained for CDX2, NANOG and T (top) or TFAP2A and OCT4 (bottom). AMLCs were generated from human ES cells by first culturing in basal medium supplemented with BMP4 for 48 h before switching to fresh basal medium for another 48 h. **h**, Transwell co-culture assays of AMLCs and human ES cells. Human ES cells were first differentiated into AMLCs by culturing on Transwell membranes in basal medium supplemented with BMP4 for 48 h. Culture medium was then switched to fresh basal medium before undifferentiated human ES cells were seeded onto Transwell membranes and co-cultured with AMLCs for another 48 h. Representative confocal micrographs show staining for CDX2, NANOG and T (top); TFAP2A, OCT4 and T (middle); E-cadherin, N-cadherin and T (bottom). **i**, Transwell co-culture assays of AMLCs and human ES cells. Human ES cells were first differentiated into AMLCs by culturing on Transwell membranes in basal medium supplemented with BMP4 (50 ng ml^{-1}) for 48 h. Culture medium was then switched to fresh basal medium before undifferentiated human ES cells were seeded onto the lower dish and co-cultured with AMLCs for another 48 h. Representative confocal micrographs show staining of cells on the lower dish for OCT4 and T (top); NANOG and T (middle); TFAP2C, NANOG and SOX17 (bottom), or cells on the Transwell membrane for TFAP2C, NANOG and SOX17 as indicated. In all immunostaining micrographs, nuclei were stained with DAPI. Boxed images show magnified views of selected areas. In **h**, insets show human ES cell colonies seeded after AMLC differentiation as marked by white arrowheads. Scale bars in **b**, **d**, **e**, 40 μm. Scale bars in **f**–**i**, 160 μm (main panels) and 10 μm (insets). Experiments were repeated three times with similar results.

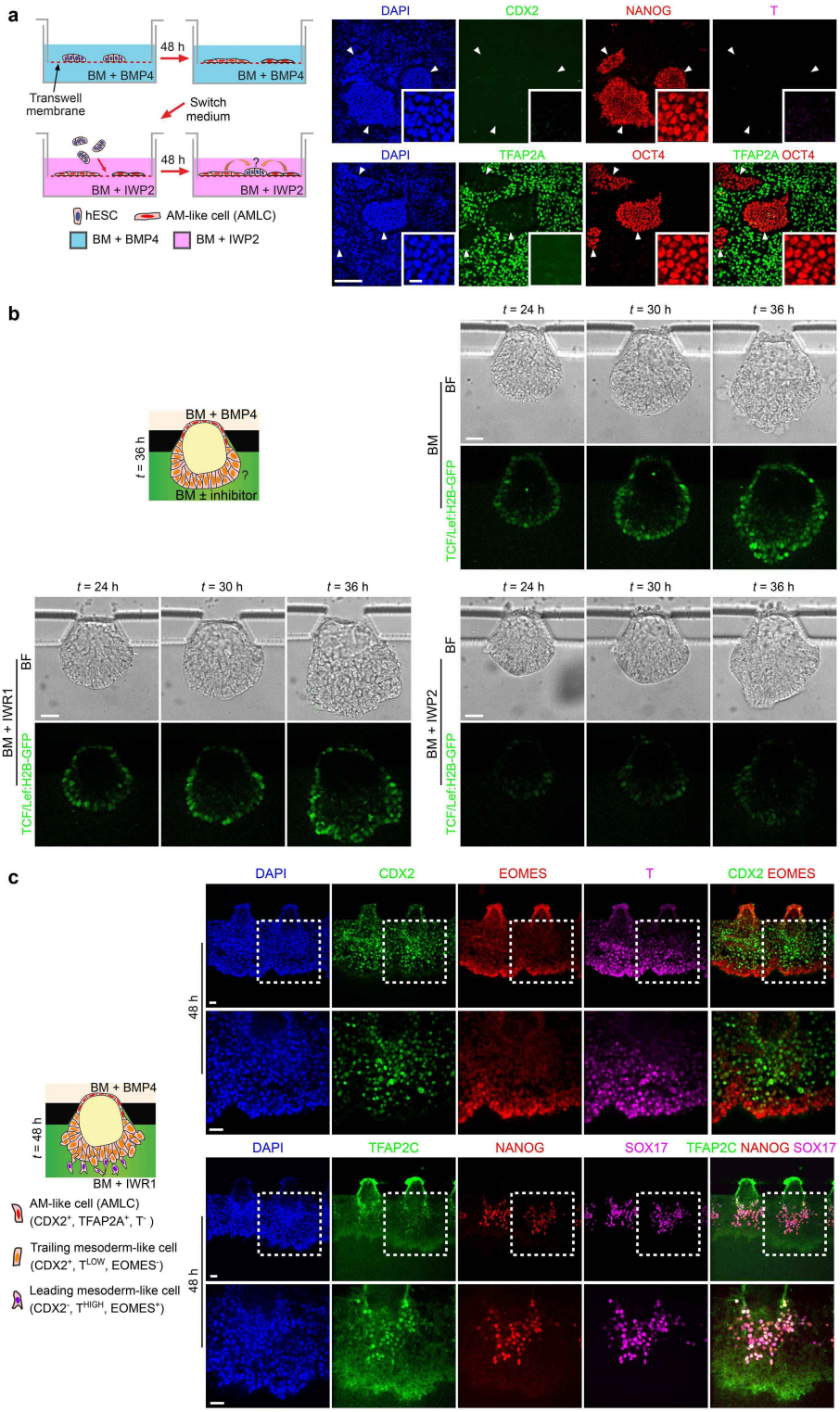

Extended Data Fig. 10 | Mesoderm induction in posteriorized embryonic-like sac is inhibited by IWP2 but not by IWR1. a, Schematic shows Transwell co-culture protocol. Human ES cells were first differentiated into AMLCs by culturing in basal medium supplemented with BMP4 (50 ng ml^{-1}) for 48 h. Culture medium was then switched to fresh basal medium supplemented with IWP2 (5 μM). At this point, undifferentiated human ES cells were seeded onto Transwell membranes and co-cultured with AMLCs for another 48 h. Representative confocal micrographs showing staining for CDX2, NANOG and T (top) or TFAP2A and OCT4 (bottom). Insets show human ES cell colonies seeded after AMLC differentiation, as marked by white arrowheads. Scale bars, 160 μm (main panels) and 10 μm (insets). **b**, Live imaging with the TCF/Lef:H2B-GFP H9 human ES cell reporter line to track Wnt–β-catenin signalling dynamics during embryonic-like sac development with or without the Wnt inhibitors IWR1 (10 μM) or IWP2 (5 μM) supplemented into the induction channel as indicated. Scale bars, 40 μm. **c**, Representative confocal micrographs show P-ELS obtained at $t = 48$ h with IWR1 (10 μM) supplemented into the induction channel as indicated. P-ELS were stained for CDX2, EOMES and T (top) or TFAP2C, NANOG and SOX17 (bottom). Outlined regions are magnified in the panel below. Scale bars, 40 μm. In **a**, **c**, nuclei were stained with DAPI. Experiments were repeated twice with similar results.

nature research

Corresponding author(s): Jianping Fu

Last updated by author(s): Jul 16, 2019

Reporting Summary

Nature Research wishes to improve the reproducibility of the work that we publish. This form provides structure for consistency and transparency in reporting. For further information on Nature Research policies, see Authors & Referees and the Editorial Policy Checklist .

Statistics

For all statistical analyses, confirm that the following items are present in the figure legend, table legend, main text, or Methods section.

n/a	Confirmed	
☐	☒	The exact sample size (*n*) for each experimental group/condition, given as a discrete number and unit of measurement
☐	☒	A statement on whether measurements were taken from distinct samples or whether the same sample was measured repeatedly
☐	☒	The statistical test(s) used AND whether they are one- or two-sided *Only common tests should be described solely by name; describe more complex techniques in the Methods section.*
☐	☒	A description of all covariates tested
☐	☒	A description of any assumptions or corrections, such as tests of normality and adjustment for multiple comparisons
☐	☒	A full description of the statistical parameters including central tendency (e.g. means) or other basic estimates (e.g. regression coefficient) AND variation (e.g. standard deviation) or associated estimates of uncertainty (e.g. confidence intervals)
☐	☒	For null hypothesis testing, the test statistic (e.g. *F*, *t*, *r*) with confidence intervals, effect sizes, degrees of freedom and *P* value noted *Give P values as exact values whenever suitable.*
☒	☐	For Bayesian analysis, information on the choice of priors and Markov chain Monte Carlo settings
☒	☐	For hierarchical and complex designs, identification of the appropriate level for tests and full reporting of outcomes
☒	☐	Estimates of effect sizes (e.g. Cohen's *d*, Pearson's *r*), indicating how they were calculated

Our web collection on statistics for biologists contains articles on many of the points above.

Software and code

Policy information about availability of computer code

Data collection	MetaMorph Advanced 7.8.1.0, AxioVision 4.8
Data analysis	Cell Ranger 3.0.0, Matlab R2011a, ImageJ 1.47t, Excel 2016, Rstudio 1.1.456, Matplotlib package in Python 1.5.2, Seurat 3.0.0.9, DAVID Bioinformatics Resources 6.8

For manuscripts utilizing custom algorithms or software that are central to the research but not yet described in published literature, software must be made available to editors/reviewers. We strongly encourage code deposition in a community repository (e.g. GitHub). See the Nature Research guidelines for submitting code & software for further information.

Data

Policy information about availability of data

All manuscripts must include a data availability statement. This statement should provide the following information, where applicable:

- Accession codes, unique identifiers, or web links for publicly available datasets
- A list of figures that have associated raw data
- A description of any restrictions on data availability

Data supporting the findings of this study are available within the article and its supplementary information files and from the corresponding authors upon reasonable request.

Field-specific reporting

Please select the one below that is the best fit for your research. If you are not sure, read the appropriate sections before making your selection.

Life sciences study design

All studies must disclose on these points even when the disclosure is negative.

Sample size	All experiments were conducted with at least two independent experiments and multiple biological replicates. Sample sizes were determined based on our previous experience and similar studies of other groups. Sample sizes were determined as sufficient since they led to similar results.
Data exclusions	Due to intrinsic inhomogeneity of Geltrex, some Geltrex continued to contract during experiments. Such experiments were excluded from data analysis. In rare cases, after initial cell seeding, concave Geltrex pockets between neighboring supporting posts could be damaged. Cell clusters formed within such damaged gel pockets were excluded from data analysis. No similar platform has been previously reported, thus the criteria were established specifically for this platform.
Replication	Reported results were repeated and confirmed for at least two independent experiments. Key experimental findings were reliably reproduced by two investigators involved in this work.
Randomization	Samples were randomly allocated to control and different experimental groups (see Methods). However, no particular randomization method was used in this work.
Blinding	Investigators were not blinded to group allocation, as no animal/human studies were conducted in this manuscript.

Reporting for specific materials, systems and methods

We require information from authors about some types of materials, experimental systems and methods used in many studies. Here, indicate whether each material, system or method listed is relevant to your study. If you are not sure if a list item applies to your research, read the appropriate section before selecting a response.

Materials & experimental systems

n/a	Involved in the study
☐	☒ Antibodies
☐	☒ Eukaryotic cell lines
☒	☐ Palaeontology
☒	☐ Animals and other organisms
☒	☐ Human research participants
☒	☐ Clinical data

Methods

n/a	Involved in the study
☒	☐ ChIP-seq
☒	☐ Flow cytometry
☒	☐ MRI-based neuroimaging

Antibodies

Antibodies used

Only certified and company-validated antibodies were used in this work:

EZRIN Mouse 1:2000 E8897 Sigma-Aldrich (Lot# 049M4838V, Clone: 3C12)
E-CADHERIN Mouse 1:500 610181 BD Biosciences (Lot# 7006620, Clone: 36/E-Cadherin)
Laminin Rabbit 1:250 ab11575 Abcam (Lot# GR202345-1, Polyclonal)
N-CADHERIN Rabbit 1:100 Ab12221 Abcam (Lot# GR139340-26, Polyclonal)
OCT4 Mouse 1:200 sc-5279 Santa-Cruz Biotechnology (Lot# B0717, Clone: C-10)
OCT4 Rabbit 1:500 2750S Cell Signaling Technology (Lot# 4, Polyclonal)
NANOG Rabbit 1:500 4903S Cell Signaling Technology (Lot# 8, Clone: D73G4)
SOX2 Rabbit 1:500 09-0024 Stemgent (Lot# J16020000000013, Polyclonal)
ZO-1 Mouse 1:1000 33-9100 Thermo Fisher Scientific (Lot# RF236801, Clone: ZO1-1A12)
GM130 Mouse 1:1000 610822 BD Biosciences (Lot# 29000, Clone: 35/GM130)
TFAP2A Mouse 1:100 sc-12726 Santa-Cruz Biotechnology (Lot# D2817, Clone: 3B5)
TFAP2C Mouse 1:100 sc-12762 Santa-Cruz Biotechnology (Lot# D2717, Clone: 6E4/4)
BRACHYURY Goat 1:100 PA5-46984 Thermo Fisher Scientific (Lot# SK2471211, Polyclonal)
BRACHYURY Rabbit 1:200 81694S Cell Signaling Technology (Lot# 1, Clone: D2Z3J)
GATA3 Mouse 1:100 MA1-028 Thermo Fisher Scientific (Lot# RL242023, Clone: 1A12-1D9)
pSMAD1/5 Rabbit 1:100 9516S Cell Signaling Technology (Lot# 9, Clone: 41D10)
SOX17 Goat 1:500 AF1924 R&D Systems (Lot# KGA0916091, Polyclonal)
CDX2 Mouse 1:300 MU392AUC Biogenex (Lot# MU392AUC Clone: CDX2-88)
EOMES Rabbit 1:200 ab23345 Abcam (Lot# GR3179448-1, Polyclonal)
BLIMP1 Rabbit 1:200 9115S Cell Signaling Technology (Lot# 6, Clone: C14A4)

The antibody information (including species, application, and catalog number) has been provided in Supplementary Information.

Validation

All antibodies have been validated by the companies from which they were purchased. The subcellular localization of all the proteins analyzed in this work is consistent with previous published literatures. This information was used to further validate the specificity. Details about validation statements of the manufacturer, relevant citations and antibody profiles can be found on the manufacturer's website.

All the antibodies utilized in this study are for immunostaining purpose. The following lists the immunostaining validation results of from the manufacturers, and the number of citations.

EZRIN (E8897): https://www.sigmaaldrich.com/catalog/product/sigma/e8897?lang=en&region=US
EZRIN (E8897) antibody was validated by the manufacturer using A431 cells. We verified that the EZRIN antibody stains apical membranes of the cystic structures exclusively, as expected. More than 40 citations.

E-CADHERIN (610181): http://www.bdbiosciences.com/eu/applications/research/stem-cell-research/cancer-research/human/purified-mouse-anti-e-cadherin-36e-cadherin/p/610181
E-CADHERIN (610181) antibody was validated by the manufacturer with WIDR cells and transfection experiments. We verified that this antibody stains the membrane of epithelial-like hPSC cysts, as expected. More than 50 citations.

Laminin (ab11575): https://www.abcam.com/laminin-antibody-ab11575.html
Laminin (ab11575) antibody was validated by the manufacturer with mouse embryos, human skins and mouse postnatal. We verified that this antibody stains the basal membrane of hPSC cysts embedded within ECM, as expected. More than 279 citations.

N-CADHERIN (Ab12221): https://www.abcam.com/n-cadherin-antibody-ab12221.html
N-CADHERIN (Ab12221) antibody was validated by the manufacturer using mouse embryos and human lung tissues. We verified that this antibody stains exclusively the mesenchyme-like cells, as expected. More than 80 citations.

OCT4 (sc-5279): https://www.scbt.com/scbt/product/oct-3-4-antibody-c-10
OCT4 (sc-5279) antibody was validated by the manufacturer using glandular cells and mouse embryos. We verified that this antibody stains the nuclei of hPSCs, as expected. More than 1151 citations.

OCT4 (2750S): https://www.cellsignal.com/products/primary-antibodies/oct-4-antibody/2750
OCT4 (2750S) antibody was validated by the manufacturer using human seminoma and NCCIT cells. We verified that this antibody stains the nuclei of hPSCs, as expected. More than 86 citations.

NANOG (4903S): https://www.cellsignal.com/products/primary-antibodies/nanog-d73g4-xp-rabbit-mab/4903
NANOG (4903S) antibody was validated by the manufacturer using human seminoma and NTERA-2 cells. We verified that this antibody stains the nuclei of hPSCs and hPGCLCs, and is negative for primitive streak-like cells, as expected. More than 102 citations.

SOX2 (09-0024): https://www.reprocell.com/antibodies-and-staining-kits-c10/stemab-sox2-antibody-affinity-purified-rabbit-anti-mouse-human-p266
SOX2 (09-0024) antibody was validated by the manufacturer using mouse ES cells. We verified that this antibody stains the nuclei of hPSCs, and is negative for primitive streak-like cells, as expected. More than 30 citations.

ZO-1 (33-9100): https://www.thermofisher.com/antibody/product/ZO-1-Antibody-clone-ZO1-1A12-Monoclonal/33-9100
ZO-1 (33-9100) antibody was validated by the manufacturer using MDCK canine cells, Caco-2 cells and brain organoids. We verified that this antibody stains the tight-junction of hPSC cysts, as expected. More than 643 citations.

GM130 (610822): http://www.bdbiosciences.com/us/reagents/research/antibodies-buffers/cell-biology-reagents/cell-biology-antibodies/purified-mouse-anti-gm130-35gm130/p/610822
GM130 (610822) antibody was validated by the manufacturer using WI-38 cells. We verified that this antibody marks the localization of Golgi apparatus, as expected. More than 30 citations.

TFAP2A (sc-12726): https://www.scbt.com/scbt/product/ap-2alpha-antibody-3b5
TFAP2A (sc-12726) antibody was validated by the manufacturer using trophoblastic cells and HeLa cells. We verified that this antibody stains the nuclei of amnion-like cells, and is negative for hPSCs, as expected. More than 40 citations.

TFAP2C (sc-12762): https://www.scbt.com/scbt/product/ap-2gamma-antibody-6e4-4
TFAP2C (sc-12762) antibody was validated by the manufacturer using human lung tumor tissues and HeLa cells. We verified that this antibody stains the nuclei of hPGCLCs, and is negative for hPSCs, as expected. More than 45 citations.

BRACHYURY (PA5-46984): https://www.thermofisher.com/antibody/product/Brachyury-Antibody-Polyclonal/PA5-46984
BRACHYURY (PA5-46984) antibody was validated by the manufacturer using mouse notochord tissues and human mesoderm-like cells. We verified that this antibody stains the nuclei of human mesoderm-like cells, and is negative for hPSCs, as expected. More than 52 citations.

BRACHYURY (81694S): https://www.cellsignal.com/products/primary-antibodies/brachyury-d2z3j-rabbit-mab/81694

BRACHYURY (81694S) antibody was validated by the manufacturer using MUG-CHOR-1 (positive) and MCF 10A (negative) cells. We verified that this antibody stains the nuclei of human mesoderm-like cells, and is negative for hPSCs, as expected. More than 4 citations.

GATA3 (MA1-028): https://www.thermofisher.com/antibody/product/GATA3-Antibody-clone-1A12-1D9-Monoclonal/MA1-028
GATA3 (MA1-028) antibody was validated by the manufacturer using MCF7 cells and SH-SY5Y cells. We verified that this antibody stains the nuclei of amnion-like cells, and is negative for hPSCs, as expected. More than 7 citations.

pSMAD1/5 (9516S): https://www.cellsignal.com/products/primary-antibodies/phospho-smad1-5-ser463-465-41d10-rabbit-mab/9516
pSMAD1/5 (9516S) antibody was validated by the manufacturer using BMP2 treated HT1080 cells. We verified that this antibody stains the nuclei of BMP4 treated hPSCs, and is negative for hPSCs, as expected. More than 164 citations.

SOX17 (AF1924): https://www.rndsystems.com/products/human-sox17-antibody_af1924
SOX17 (AF1924) antibody was validated by the manufacturer using B16 mouse cells and endoderm-like cells differentiated from BG01V human embryonic stem cells. We verified that this antibody stains the nuclei of hPGCLCs, and is negative for hPSCs, as expected. More than 119 citations.

CDX2 (MU392AUC): http://store.biogenex.com/us/applications/ihc/controls/controls/anti-cdx-2-clone-cdx2-88.html
CDX2 (MU392AUC) antibody was validated by the manufacturer using intestine tissues. We verified that this antibody stains the nuclei of amnion-like cells, and is negative for hPSCs, as expected. More than 30 citations.

EOMES (ab23345): https://www.abcam.com/tbr2-eomes-antibody-chip-grade-ab23345.html
EOMES (ab23345) antibody was validated by the manufacturer using mesendoderm cells differentiated from human embryonic stem cells. We verified that this antibody stains the nuclei of mesendoderm-like cells, and is negative for hPSCs, as expected. More than 270 citations.

BLIMP1(9115S): https://www.cellsignal.com/products/primary-antibodies/blimp-1-prdi-bf1-c14a4-rabbit-mab/9115
BLIMP1(9115S) antibody was validated by the manufacturer using SR cells (positive) and HeLa cells (negative). We verified that this antibody stains the nuclei of hPGCLCs , and is negative for hPSCs, as expected. More than 36 citations.

Eukaryotic cell lines

Policy information about cell lines

Cell line source(s)	The following cell lines were used in this work: H9 hESC line (WA09, WiCell; NIH registration number: 0062); H1 hESC line (WA01, WiCell; NIH registration number: 0043); A hiPSC line (1196a) originally reported in Villa-Diaz, L. G. et al. Nat. Biotechnol. 28, 581 (2010).
Authentication	All hPSC lines have been authenticated by the original sources and also authenticated in-house by immunostaining for pluripotency markers and successful differentiation to the three germ layer cells.
Mycoplasma contamination	All cell lines used in this work have been tested negative for mycoplasma contamination.
Commonly misidentified lines (See ICLAC register)	No commonly misidentified cell lines listed by ICLAC were used in this work.